reactions

MDPI

Review

Carbon Nanotubes: A Review of Synthesis Methods and Applications

Arash Yahyazadeh [1], Sonil Nanda [2] and Ajay K. Dalai [1,*]

[1] Department of Chemical and Biological Engineering, University of Saskatchewan, Saskatoon, SK S7N 5A9, Canada; ary977@usask.ca
[2] Department of Engineering, Faculty of Agriculture, Dalhousie University, Truro, NS B2N 5E3, Canada; sonil.nanda@dal.ca
* Correspondence: ajay.dalai@usask.ca; Tel.: +1-306-966-4771

Abstract: Carbon nanotubes (CNTs) are cylindrical-shaped materials composed of hexagonally arranged hybridized carbon atoms with versatility in synthesis methods and diverse applications. This review is focused on the fabrication, physicochemical and spectroscopic characterization, and industrial applications of CNTs. This review discusses some promising synthesis methods for the preparation of CNTs such as catalytic chemical vapor deposition, arc discharge, and laser ablation. A comparative discussion is made between these synthesis methods in terms of strengths, opportunities and challenges. Furthermore, functionalization and purification of CNTs' surface leading to improved functionality has also been highlighted in this article. Finally, the analytical techniques employed to shed light on the physicochemical and morphological properties of CNTs are described.

Keywords: carbon nanotubes; synthesis; application advances; characterization; surface modifications

check for updates

Citation: Yahyazadeh, A.; Nanda, S.; Dalai, A.K. Carbon Nanotubes: A Review of Synthesis Methods and Applications. *Reactions* **2024**, *5*, 429–451. https://doi.org/10.3390/reactions5030022

Academic Editors: Annalisa Volpe, Caterina Gaudiuso and Maria Chiara Sportelli

Received: 1 May 2024
Revised: 10 June 2024
Accepted: 2 July 2024
Published: 4 July 2024

Copyright: © 2024 by the authors. Licensee MDPI, Basel, Switzerland. This article is an open access article distributed under the terms and conditions of the Creative Commons Attribution (CC BY) license (https://creativecommons.org/licenses/by/4.0/).

1. Introduction

Since being reported in 1991, carbon nanotubes (CNTs) are well known for their exceptional morphological, physical, electrical, thermal, and magnetic properties [1]. CNTs are cylindrical-shaped carbon fibers materials composed of hexagonally arranged hybridized carbon atoms with diverse industrial applications. Based on their structural features, CNTs can be broadly categorized into single-walled CNTs (SWCNTs), double-walled CNTs (DWCNTs), and multi-walled CNTs (MWCNTs). Some of the chief physicochemical properties of CNTs are summarized in Table 1.

Mass production of CNTs and high-volume applications of CNTs open a new perspective in nanomaterials and nanodevices. The chirality of a nanotube is typically described in terms of two integers (n and m), which determine the structure of tubulenes. As shown in Figure 1, the achiral tubulene divided the so-called zig-zag nanotubes and armchair nanotubes. Armchair (2,2) (Figure 1a) and zigzag (4,0) (Figure 1b) configurations play a crucial role due to interlayer van der Waals forces. The unit cells differentiate these groups and determine the electronic–optical properties of nanotubes. It has been predicted that CNTs can be employed as either a metallic or as semiconductors due to their optical properties. As shown in Figure 1, in ac doping and zz doping, the axis of the tube is parallel and perpendicular to the carbon–carbon bond. Detailed investigation of dynamic behavior using atomistic model-based simulation indicates that the zigzag form of CNTs is more sensitive as compared to ac doping [2]. The ground state geometries of zigzag and armchair configurations conclude that CNTs can act as electro–optic modulators [3].

Table 1. Physical properties and unique structure of SWCNTs and MWCNTs.

Properties		SWCNTs	MWCNTs	Remarks
Mechanical features	Young's modulus	~1 TPa	~1–1.2 TPa	Approximately five-times tougher than steel
Mechanical features	Tensile strength	~60 GPa	~0.15 TPa	Approximately one-hundred-times tougher than steel
Electronic features	Bandgap	When n-m is divisible by 3 (0 eV, metallic)	~0 eV (non-semiconducting)	Excellent electrical and thermal conductivity, current carrying capacity, and strength
		When n-m is not divisible by 3 (0.4–2 eV, semiconducting)		
Thermal features	Thermal conductivity at ambient temperature	1750–5800 W/mk	>3000 W/mk	Approximately three-times better than diamond
Electrical features	Typical resistivity	10^{-6} Ω m		Remarkable conductivity due to the nanostructures and strength of carbon bonds
	Typical maximum current density	10^{7}–10^{9} A cm^{-2}		
	Typical quantized conductance	12.9 kΩ^{-1}		

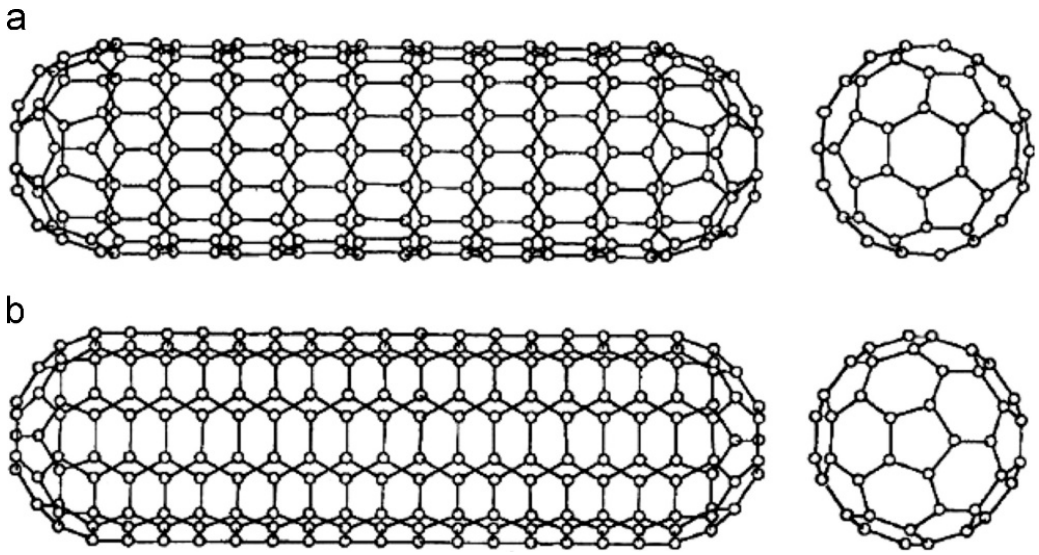


Figure 1. Illustration of the monolayer nanotubes. (**a**) Armchair and (**b**) zigzag. Reproduced with permission [4].

Singh et al. studied the electronic and mechanical properties of (6,1) SWCNT with periodic doping of Boron atoms. Armchair (ac) doping and zigzag (zz) doping patterns show higher stability. Figure 2 shows the effect of B doping in the tensile response which corresponds to the fracture point. Increasing the dopant concentration with an ac pattern and zz doping leads to significant drops in the tensile response. Young's moduli values based on the strain–stress graph confirm values in the range of 1.38 ± 0.1 TPa for the ac doping pattern [5].

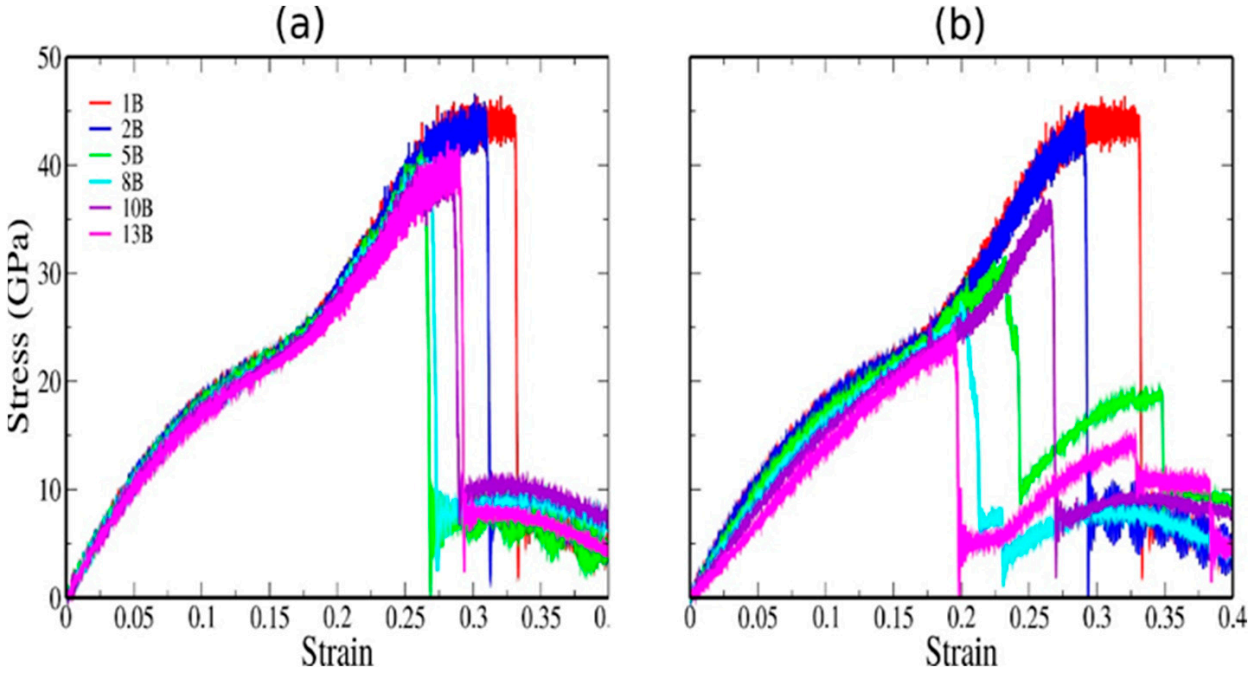


Figure 2. The strain–stress behavior for (**a**) ac doping and (**b**) zz doping. Reproduced with permission [6].

CNTs open possibilities for applications including drug delivery in medicine, data storage devices, and lithium-ion batteries. Additionally, CNTs have extraordinary mechanical characteristics, high thermal properties, and excellent optical properties. The major challenge for the application of CNTs in drug delivery is the toxicity of CNTs which limits commercialization in the market [7]. Additionally, the polymer–CNT network is found to increase the gas flow for endless applications such as in the electronics industry. Chemical modification of CNTs including covalent and noncovalent functionalization results in the application of CNTs in the removal of dyes from wastewater. To optimize functionalization of CNTs, which affects the CNT surface armature parameters such as operating temperature and presence of the catalyst, need to be considered. The large-scale production of CNTs, controlling the growth of nanotubes, and the number of impurities are some important challenges that need to be answered [8].

2. Methods of the Synthesis of CNTs

CNTs can be prepared using methods such as arc discharge, catalytic chemical vapor deposition (CCVD), laser ablation, and gas-phase pyrolysis. Each of these techniques affects the application of the developed CNT due to their semiconducting or metallic nature. Among the different techniques for the development of CNTs, the CCVD process seems to be more adapted for large-scale production at lower cost with minimal impurities and of a certain chirality [9]. Figure 3 shows the schematic diagram of the available techniques for the preparation of CNTs. Each of the synthesis methods establishes the relationships between the weight and the density of CNTs. The different methods shown in Figure 3 have specific capabilities, efficiencies, and possible exploitation in economic large-scale synthesis.

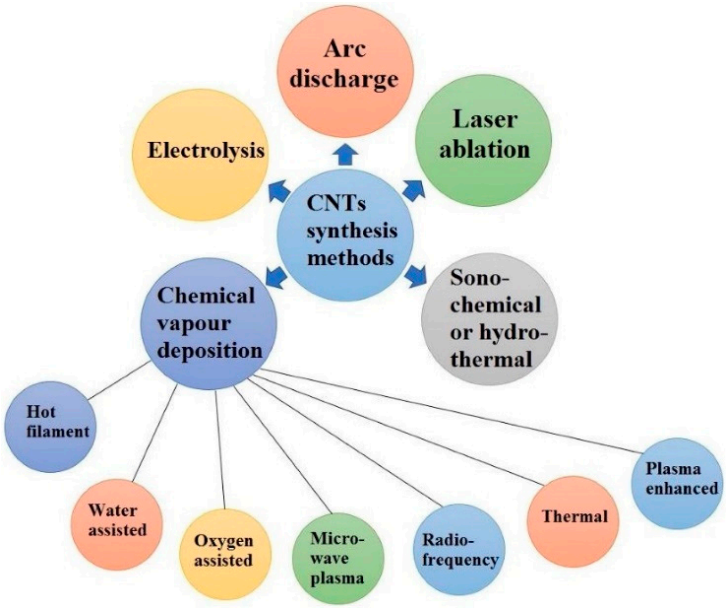


Figure 3. Synthesis methods of CNTs. Reproduced with permission [10].

2.1. Arc Discharge Method

The arc discharge method in typically carried out in an inert environment with high-temperature discharge between two electrodes (Figure 4). In arc discharge, the chamber anode is filled with a carbon precursor and the cathode is a pure graphite rod. During the process, a constant current is maintained to produce high-quality CNTs at a high temperature of ~4000–6000 K. Large-scale synthesis of CNTs is contingent upon the thermal energy of the plasma or high heat flux. Maria and Mieno [11] reported on the use of a bipolar pulsed arc discharge method for the preparation of CNTs. It was shown that the bipolar pulsed arc discharge tends towards the production of SWCNTs. Raniszewski et al. [12] conducted a technical evaluation of MWCNTs' production in arc discharge systems. They observed that the lower plasma jet temperature is responsible for the size and structure of the carbon. The arc discharge process is strongly affected by various synthesis parameters such as voltage, arc current, and frequency. Bagiante et al. [13] found that the mechanical properties of CNTs synthesized using the arc discharge method depend on the current and electrode diameter. Moreover, by improving the surface area of the cathode, longer nanotubes with a lower amorphous structure can be obtained.

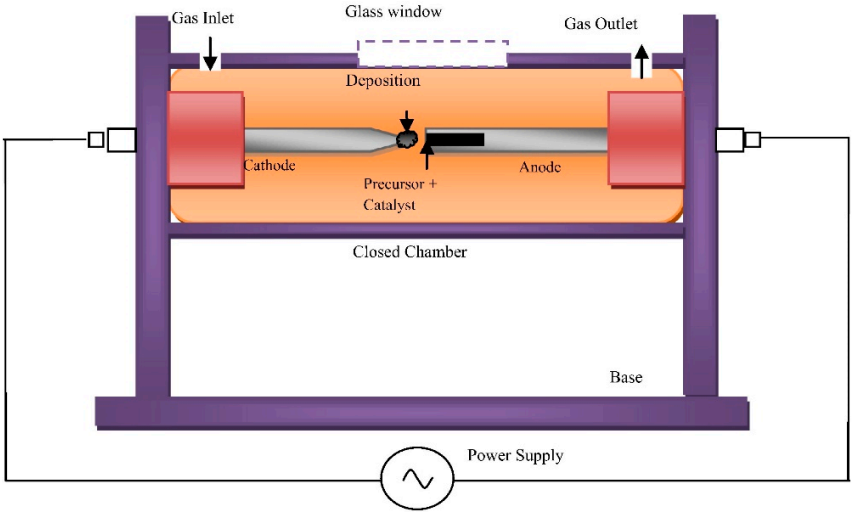


Figure 4. Schematic representation of arc discharge and CNT formation. Reproduced with permission [14].

The arc discharge process is reliant on variables such as plasma power, arc current, catalyst, and electrode geometry [14]. The catalyst effect in the synthesis of CNTs is shown in Figure 5. The size of CNTs can be affected by using the proper size of metal catalyst particles. Furthermore, the composition of catalyst particles plays an important role in the yield of CNTs. The metal particles encapsulate carbon vapors to form SWCNTs.

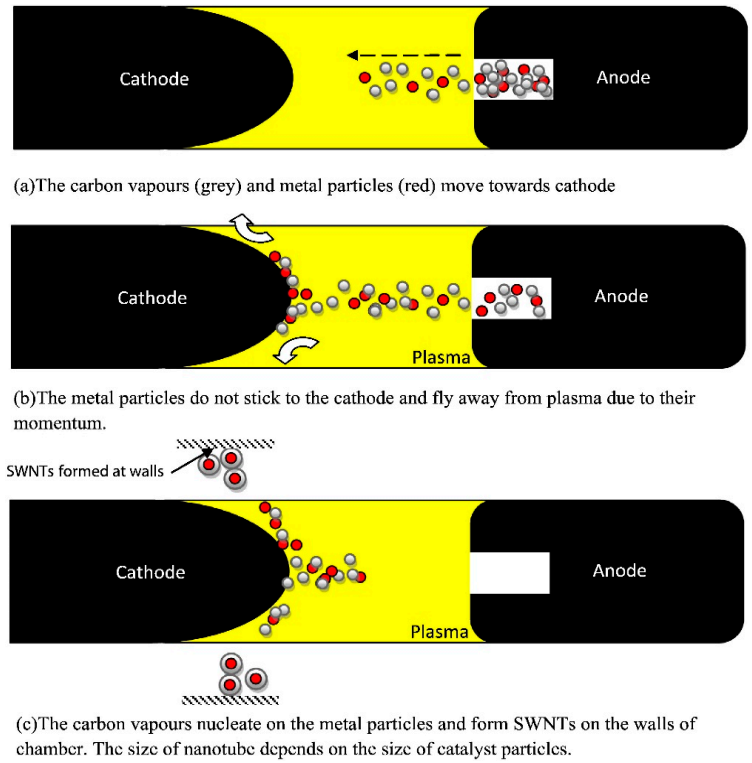


Figure 5. Graphical representation of the role of the catalyst in synthesizing CNTs via the arc discharge method. Reproduced with permission [14].

2.2. Catalytic Chemical Vapor Deposition Process

In the CCVD process, transition metals are employed for the dissociation of hydrocarbon molecules at high temperatures (500–1000 °C). Zhang et al. [6] stated the production of CNTs on surface of biochar via microwave-assisted chemical vapor deposition (CVD) method using an Ni-based catalyst. They observed that the CNTs synthesized at 600 °C were multiwalled with a d-spacing of 0.34 nm. The synthesis of CNTs was conducted in a self-designed quartz reactor using CH_4 (60 vol%) as the carbon source. Awadallah et al. [15] produced CNTs using the CCVD technique over Ni-Mo and Co-Mo supported on alumina catalysts at 700 °C (Figure 6). In the CVD reactor, the first step is to synthesize metal nanoparticles on a support. In the pretreatment step, under typically hydrogen or NH_3, the nanoparticles are formed. Finally, hydrocarbon gas (NG) is let into the furnace and carbon deposition happens through catalytic decomposition of the hydrocarbon molecules on the metal nanoparticles between 500 and 1200 °C. Using CVD synthesis, the CNTs' growth mechanism can be different, reliant on the interactions between the catalytic material and the substrate (Figure 7). The oldest method for CNT production is electric arc discharge, and other methods including laser ablation and CVD techniques are different in terms of the quality and purity of the obtained products. The arc discharge technique uses different aromatic hydrocarbons as carbon feedstock and the best quality CNTs are obtained when a mixture of ferrocene–nickelocene is used as the catalyst. The physical and chemical parameters including temperature, catalyst composition, and presence of H_2 influence CNTs' inner and outer diameters. It was reported that the growth mode changes from tip-growth (Figure 7a) for large particles (>>5 nm) to base-growth (Figure 7b) for smaller ones (<5 nm). The difference between the growth mode is explained by the adhesion force

between the catalyst and the support. The catalytic growth mode, including base-growth and tip-growth mechanisms, is explained in terms of adhesion force between the catalyst and the support. It was reported that there is a strong correlation existing between catalyst particle size and the growth mode in carbon structuring into CNTs. Moreover, tip-growth is the active mode for CNT growth from large particles as for cobalt- and nickel-grown CNTs. It was concluded that the adhesive force is proportional to the contact area, and interconnected catalyst islands results in base-growth [16]. In another study, it was shown that the growth mode can be changed from tip to base growth through plasma pretreatment of the catalyst. The correlation between the CNT size and the growth mode was studied using iron deposited on the silicon without any oxide intermediate layer. TEM images confirm metallic particles are diffused inside the tip of CNTs with plasma treatment of the catalyst before growth. On the other hand, to determine the growth direction a clear conjunction line is observed, indicating that the growth front is at the base of the forest. It is demonstrated that with the plasma pretreated catalyst, oxidation of the catalyst is required to induce the base-growth mode. Furthermore, the difference in the CNT size can be described by nucleation conditions and difficulty of nucleation for small diameter tubes. The Ellingham diagram attributed to the metal nucleation in the oxide phase is in agreement with the observed tube diameter and structures. It was concluded that the particle diameter is not the key factor which determines the growth mode, and the chemical state of the catalysts plays an important role [17].

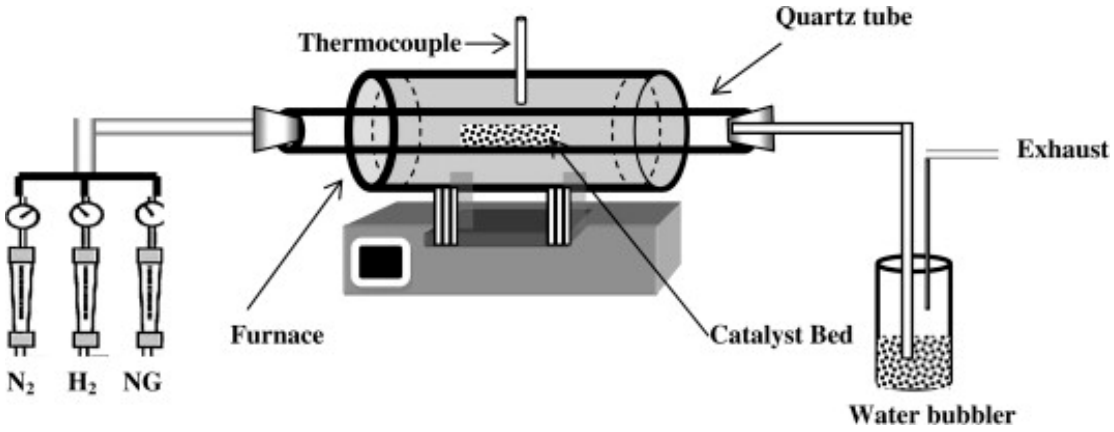


Figure 6. A typical schematic diagram of CCVD for the synthesis of CNT using methane. Reproduced with permission [15].

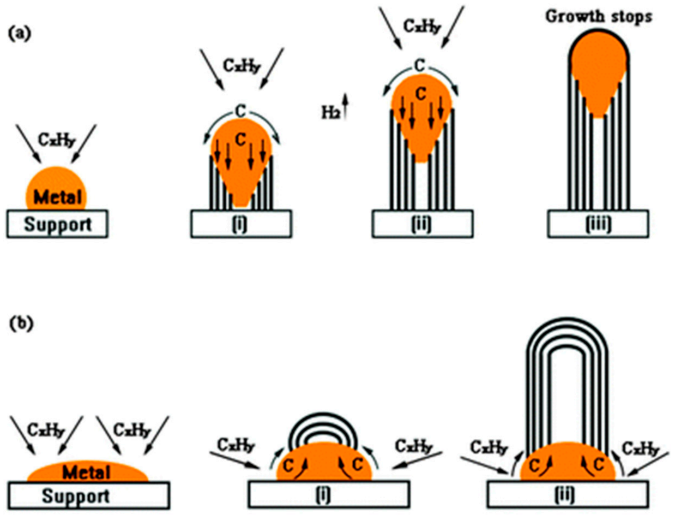


Figure 7. (**a**) Tip-growth model and (**b**) base-growth model for the growth of CNTs. Reproduced with permission [18].

Considering using the bimetallic catalyst in the CCVD process, Rattanaamonkulchai et al. [19] used a series of bimetallic FeMo/MgO, NiMo/MgO, and CoMo/MgO catalysts for the synthesis of CNTs and hydrogen from biogas. CoMo/MgO and NiMo/MgO achieved a remarkable yield of hydrogen and CNTs. Moreover, TGA plots of the synthesized CNTs indicated that molybdenum addition can reduce the defect structure or amorphous carbon. Considering the optimization of synthesis parameters for CNTs' growth, Bankole et al. [20] investigated an Fe-Co/ $CaCO_3$ catalyst. They suggested that the key synthesis parameters to maximize the yield of CNTs are stirrer speed and loading of support. The Fe-Co bimetallic catalyst preparation factors, including drying time, calcination temperature, stirring speed, and support weight, were studied for optimizing the yield and quality of synthesized CNTs. Stirring speed changed from 1000 to 2000 rpm, and it guarantees homogenous mixing and dispersion of the metal particles on the support. It was reported that there was a direct linear relationship between the catalyst yield and stirring speed, resulting in improved chemical bonds. Table 2 shows the yield of CNTs using different carbon sources with CCVD on a supported catalyst. The CVD technique offers a controllable process for the selective production of CNTs using the catalytic decomposition of hydrocarbon or CO feedstock. The general CNT growth mechanism in the CVD process is the precipitation of carbon from the metal particle depend on the working conditions. The commonly used thermal CVD produces aligned MWNTs and SWNTs on different substrates such as Ni, Si, SiO_2, Cu/Ti/Si, stainless steel, and glass. The alcohol-CVD technique is used for producing high-purity SWNTs using different metal rods (Ni, Ni/Co, and Fe). The synthesis of CNTs with the alcohol-CVD technique using copper has already been demonstrated.

Table 2. Different catalysts used in the synthesis of CNTs via the CCVD method.

Catalyst	Reaction Conditions	CNTs Yield (%)	Reference
Fe	Reaction temperature (800 °C), argon flow rate (150 cm^3/min), carbon source and catalyst (Ferrocene (2 wt%) in toluene with a rate of 0.14 mL/min), deposition time (30–180 min)	The yield was not determined.	[21]
Silicon wafers coated with a catalyst film of Fe/Co	Reaction temperature (700 °C), ammonia in a gas mixture of argon (75 mL/min), deposition time (20 min to 2 h), carbon source (mixture of acetylene and pyridine)	The yield was not determined.	[22]
Fe-Mo-MgO	Reaction temperature (850 °C), argon flow rate (100 mL/min), mass of catalyst (100 mg), deposition time (30–45 min), carbon source (ethanol)	The CNT yield increased with synthesis time.	[23]
Fe-Cr on Si substrate	Reaction temperature (825 °C), argon flow rate (100 sccm), deposition time (15 min), carbon source (liquid petroleum gas)	The yield was not determined.	[24]
Fe-Co-Ni on a $CaCO_3$ substrate	Reaction temperature (600–750 °C), argon flow rate (40 sccm), deposition time (30 min), carbon source (C_2H_2)	Mass of carbon deposited (0.36–0.78 gm/gm).	[25]
Fe-Co on the surface of Al substrate	Reaction temperature (640 °C), carbon source (ethylene) nitrogen flow rate (50–75 sccm), reaction time (2–30 min)	The yield was not determined.	[26]

2.3. Laser Ablation Method and Other Techniques

This method can result in synthesizing SWCNTs with high purity and quality. Zhang et al. [27] produced SWCNTs using bimetal NiCo and NiFe catalysts using laser ablation at 1200 °C for 1 h. Their study indicated that increasing the loading of Fe resulted in a higher diameter of the produced SWCNTs. Raman spectroscopy showed that the SWCNT yield remained almost unchanged for an Fe concentration of up to 0.5%. Zhang et al. [28] used a continuous-wave CO_2 laser ablation method by varying the laser power from 500 W to 850 W to produce SWCNTs. The yield of SWCNTs was estimated to be approximately 70% with the diameter of SWCNT bundles ranging from 6 to 20 nm. The intensities of Raman breathing mode peaks suggested the successful synthesis of

SWCNTs, although it varied with the laser power. Bota et al. [29] studied a laser ablation chamber for SWCNT production using small amounts of metallic catalyst. CNTs with a diameter of 1.4 nm embedded within the amorphous carbon were observed through the transmission electron microscopy (TEM) and high-resolution transmission electron microscopy (HRTEM) imaging (Figure 8). Figure 8 shows that Pt-Co as the catalyst produced amorphous carbon and SWCNTs. Diameters of individual SWCNTs have been measured between 1.2 and 1.5 nm and higher purity of SWCNTs is achieved with a concentration of 0.6 at-%Co and 0.6 at%Ni. It was concluded that a longer quartz tube could lead to higher (70%) production of SWCNTs.

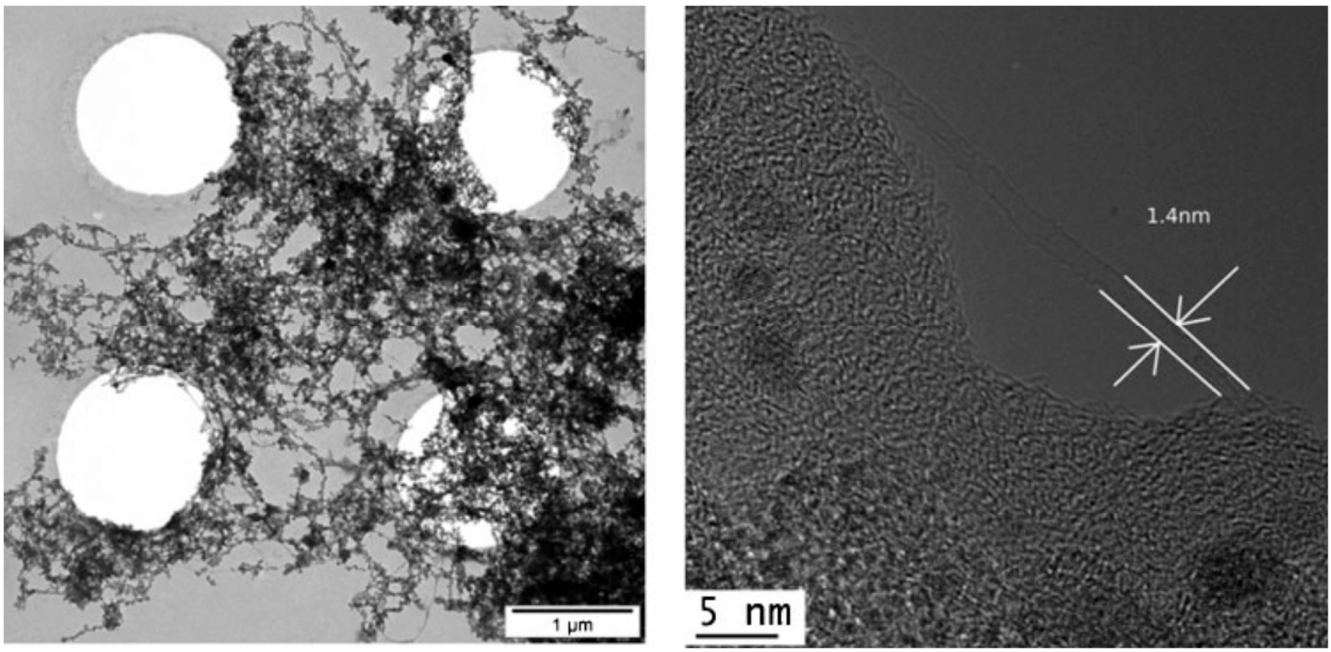


Figure 8. TEM and HRTEM images of ablation products representing the network of SWCNT bundles and amorphous carbon. Reproduced with permission [29].

Yuge et al. [30] reported on the production with a higher yield of crystalline MWCNTs using continuous-wave mode CO_2 laser ablation at room temperature. Hameed et al. [31] reported on the preparation of a graphene sheet and different carbon nanomaterial pore diameters ranging from 7 to 16 nm by varying the laser energy in the laser ablation of a carbon target in liquid. The pulsed laser ablation technique leads to the best purity and yield of SWCNTs, which appear to be entangled threads with lengths of several hundred micrometers. The higher laser intensity and higher furnace temperature correspond to the highest SWNT yield.

Tabatabaie and Dorranian [32] developed a laser ablation technique with graphite in liquid nitrogen to generate carbon nanostructures and graphene nanosheets. A significant amount of graphene nanosheets were synthesized in the case of the products at lower laser fluence. Carbon nanoparticles and fluorine were generated with a laser fluence higher than 1.1 J/cm^{2}a. Mwafy and Mostafa [33] reported that an SnO_2/MWCNTs nanocomposite structure can be used as an adsorbent for efficient removal of Cu(II) from wastewater. As depicted in Figure 9, SnO_2/MWCNT nanocomposite was synthesized using pulsed laser ablation, and it showed high adsorbing efficiency at a pH value of 5.7. It was shown that the efficacy of the adsorption capacity increases with the increasing concentration of copper until reaching saturation of the surface with copper ions. The used laser parameters are 1064 nm wavelength, 7 ns pulse width, and 10Hz repetition rate. The prepared suspension nanocomposite from MWCNTs and SnO_2 was located in a plastic filter holder, and thermal treatment was carried out for 2 h under a nitrogen atmosphere at 300 °C.

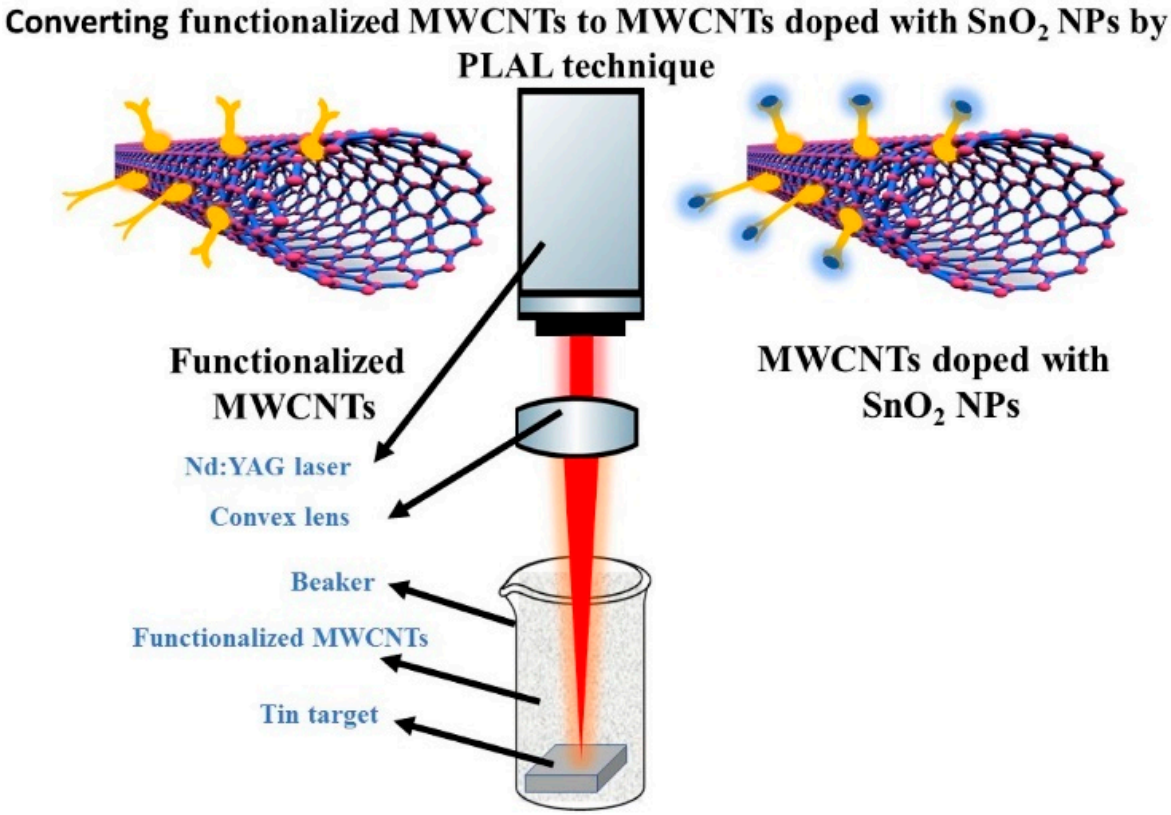


Figure 9. Preparation of SnO_2/MWCNTs nanocomposites. Reproduced with permission [33].

The sonochemical/hydrothermal method is used for the synthesis of nano-onions, nanorods, and MWNTs from several to more than 100 carbon layers. The hydrothermal technique produces CNTs about 60 nm in diameter, 2–5 μm long, and with internal cavities with diameters from 10 to 80 nm.

Electrolysis uses electrowinning of alkaline-earth metals on a graphite cathode for nanotube production in fused NaCl at 810 °C using argon as an inert gas. MWCNTs prepared this way exhibit diameters of 10–20 nm and a length of 500 nm using the process of cathodic reduction of CO_2 to elemental carbon on metallic electrodes.

The solar technique is used for SWNT production in gram quantities using a 50 kW solar reactor and an Ni-Co catalyst. The quality of the produced material was influenced by the vaporization temperature which remained in the range 2627–2727 °C [34].

3. Common Characterization Techniques for CNTs

Popular techniques such as atomic force microscopy (AFM), contact angle, thermogravimetric analysis (TGA), X-ray diffraction (XRD), TEM, X-ray photoelectron spectroscopy (XPS), and Fourier transform infrared (FT-IR) and Raman spectroscopy are used to characterize the structure and chemical composition of CNTs (Table 3). Teimuri-Mofrad et al. [35] reported that the FT-IR spectra confirmed the chitosan (Cs)–ferrocene (Fs) moieties have successfully been functionalized on CNTs. According to the XPS studies of SWCNTs with phthalocyanines, there is a strong interaction between macrocyclic complexes and CNT sidewalls. It was shown that the transition metal spectra correspond to a single oxidation state in zigzag-shaped nanotube-bound complexes [36]. TEM imaging of CuO/ZnO/CNTs thin films confirm a nanocrystalline and densely packed microstructure [37]. The proliferation of CNTs was independent of temperature since individual monolayers were observed. Recently, Li et al. [38] reported that the Raman shift during deformation of the carbon-based materials leads to the expanding and splitting of the G band. Raman spectroscopy of CNTs can also detect defects in the carbon structures including edges, grain boundaries, and

cracks. Generally, characterization devices are employed for different studies of CNTs based on their application perspective. Mechanical properties of CNTs, such as Young's modulus, are measured with tensile testing. Furthermore, thermal properties of CNTs are dependent on the temperature and can be measured with TGA. Functionalization of CNTs have made them soluble in water which plays a pivotal role in biomedical applications. The FT-IR technique is used for determining the various types of functional groups on CNTs which result in the reactivity of the surface and dispensability of CNTs. Techniques such as UV-NS are employed for measuring CNTs' chirality and concentration for analyzing a few aspects of CNTs' dispersion. HRTEM analysis can assess the purity of CNTs and their growth mechanisms. Additionally, the structure and pore size distribution of the CNTs, including inner pore accessibility and the external diameter, can be revealed using TEM.

Table 3. Common characterization techniques for CNTs.

Characterization Technique	Main Purpose	Reference
Atomic force microscopy	Surface roughness and topographies display small bumps of wrinkled materials.	[39]
Contact angle	The super-oleophilic characteristics of the as-prepared CNT aerogel.	[40]
Thermogravimetric analysis	The thermal stability of reinforced microencapsulated phase change materials with CNTs.	[41]
X-ray diffraction	The interplanar dividing and structure of MWCNTs.	[42]
X-ray photoelectron spectroscopy	Characterize the chemical composition of the composite and approve the presence of Ag nanoparticles in the CNTs.	[43]

4. Applications of CNTs

4.1. Applications of CNTs in Pharmaceutical

A wide range of applications for CNTs with their unusual structure and properties including extremely high surface area, remarkably high mechanical strength, and relative chemical inactivity have been reported in the literature. Peretz and Regev [44] reviewed CNTs' application in the biomedical industry and CNT-based nanocarriers in drug delivery. Figure 10 shows CNT conjugation with Doxorubicin as a well-known anticancer drug. The CNTs' large diameter leads to low cell uptake efficiency and enhances adsorption via Π-Π stacking. The dissociation of Doxorubicin loaded onto the surface of SWCNT occurs in acidic environments at the tumor sites [45]. It has been concluded that the toxicity issue of CNTs still awaits a consensus for their successful use as nano-carriers. The aromatic rings successfully deposited onto the surface of PEGylated SWCNTs at the tumor sites, which are slightly acidic (Figure 10A). A triple functionalization of oxidized SWCNTs using two binding methods attach the fluorescent marker and the antibodies (Figure 10B). For SWCNTs changed by polysaccharides on human cervical carcinoma cells, SWCNTs accumulate in the tissues (Figure 10C). Conjugated PTX to coated SWCNTs can reduce tumor volume owing to the higher tumor uptake of the SWCNT–PTX (Figure 10D).

Wang et al. [46] later reported that functionalized MWCNTs coiled into helical fiber bundles can be employed as electrochemical sensors to detect Ca ions and glucose in blood samples. The authors presented different electrochemical sensors to identify ions and prostate-specific antigens, suggesting that CNTs can be used as modern implantable tissues. The applications of CNTs in pharmacy and medicine are summarized in Table 4.

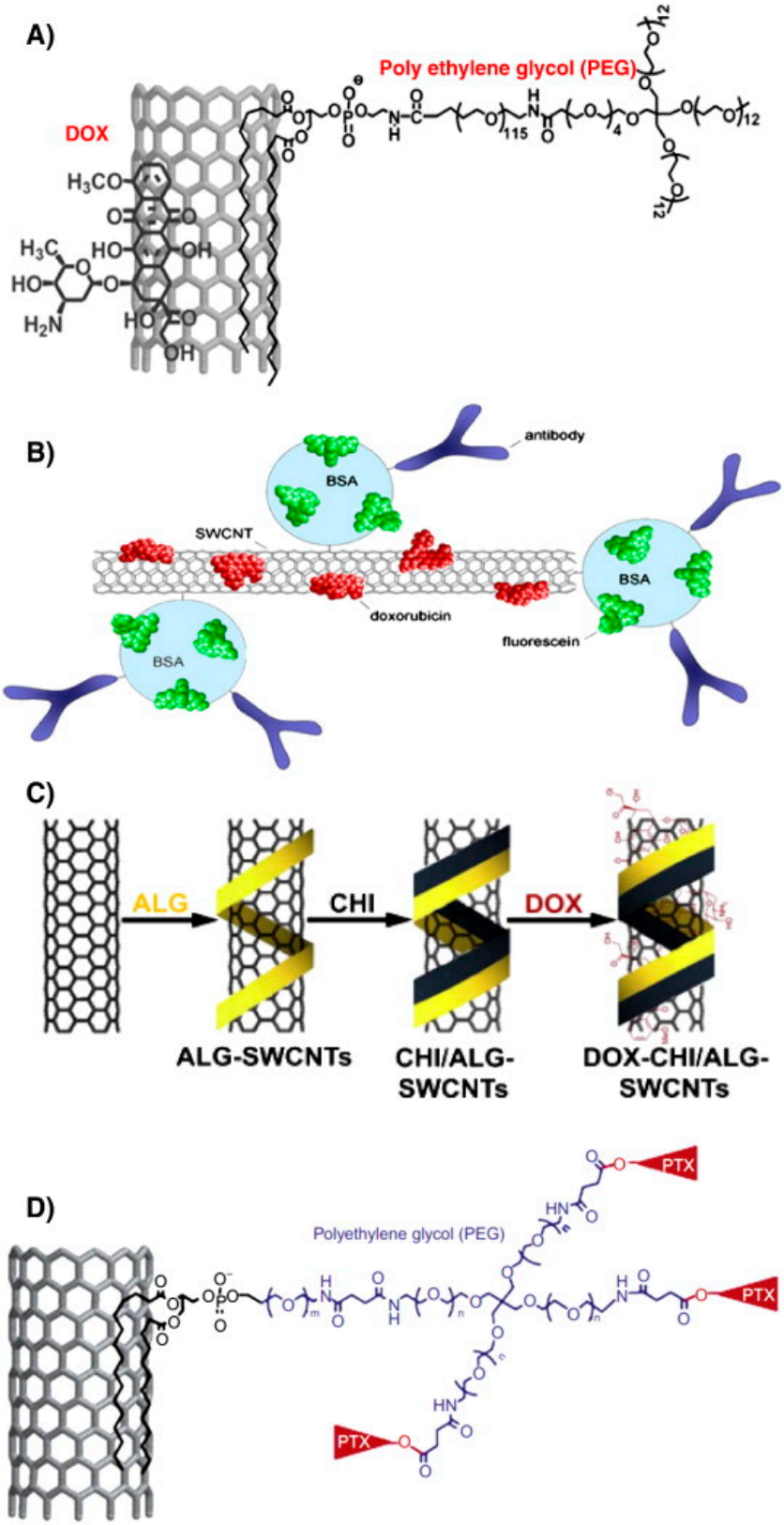


Figure 10. CNT conjunction with Doxorubicin (DOX): (**A**) Polyethylene glycol (PEG) loaded by Doxorubicin via supramolecular. (**B**) Doxorubicin–antibody conjugate. (**C**) SWCNTs conjugate with alginate sodium (ALG), chitosan (CHI), and Doxorubicin. (**D**) Paclitaxel (PTX) linked to PEG–SWCNT. Reproduced with permission [44].

Table 4. Applications of CNTs in pharmaceutical research and development.

Applications	Preparation Method	CNTs Type and Dimensions	Remarks	Reference
Using CNT-based 3D scaffold for regenerative medicine	CVD method	Outer diameter of 10–20 nm and 150–200 μm long	CNTs with bacterial cellulose are proper for use as a bone graft material	[47]
Using CNT yarns–gold particles–polymer composites for ultrasound application	CVD spinning process	CNT with a thickness of 5 μm	CNT yarns are promising structures for drug delivery applications	[48]
Functionalized SWCNTs in mice bone marrow cells	CCVD technique	Outer diameter of 1.5–3 nm and 15–20 μm long	Interaction between CNTs and deoxyribonucleic acid (DNA) helps to understand the chemical toxicity in bone marrow	[49]
MWCNTs lead to rapid colonization of the lungs	Commercially available MWCNTs	Average length of 20–50 μm	Enhanced tumor angiogenesis was observed in the CNT-exposed group	[50]
SWCNTs as nanomedicine therapies in cancer cell killing	-	-	Due to absorbing electromagnetic waves, SWCNT paves the way for novel therapeutic approaches	[51]
Amin-functionalized SWCNTs for bone tissue engineering	Commercially available SWCNTs	200–800 nm diameter	The addition of SWCNTs enhanced the proliferation of the bone marrow-derived mesenchymal stem cells	[52]

Due to surface structure and the high sensitivity of the electronic properties of nanotubes, CNT is a promising superminiaturized chemical and biological sensor [4]. Ni-Co nanowire-filled MWCNTs were designed with superior stability and reasonable cost for detecting glucose [53]. Furthermore, Ni-Co/MWCNT nanocomposite preserved the synergistic and intrinsic electrical conductivity while showing excellent selectivity against reducing sugars in human blood. Some applications of CNT sensors and probes are summarized in Table 5.

Table 5. Applications of CNTs nanoprobes and sensors in nanoelectronics.

Applications	Preparation Method	CNT Type and Dimensions	Remarks	Reference
Polymer-dispersed liquid crystal doped with CNTs used as a gas sensor	Commercially available MWCNTs	10–20 nm in diameter and 1–2 μm in length	The selectivity of the proposed acetone gas sensor can be detected by measuring the variations in the electrical resistance of the sensing film.	[54]
MWCNT–ionic liquid–carbon paste electrode for determination of mercury ions (II)	Commercially available MWCNTs	10–40 nm diameters and 1–25 μm length	Using MWCNTs in the composition of the carbon paste improved the response time of the sensor.	[55]
Cu-nanoparticles on MWCNTs used for enzyme-free sensors in the oxidation of glucose	Commercially available MWCNTs	60–80 nm of outer diameter and 10–15 μm of average length	Electrochemical measurements confirmed high sensitivity and fast response time due to the synergetic effects of combining copper with CNTs.	[56]

Confining metal-based nanoparticles into CNTs can be employed for electrochemical energy conversion and storage devices. The confinement of metal into CNTs leads to an electron potential difference between the inner and outer walls of CNTs [57]. Xue et al. [58]

fabricated $NiCo_2O_4$ nanoparticles on CNTs as the materials for electrodes used in high-performance supercapacitors. The electrochemical performances at various scan rates confirmed that DNA addition enhanced the $NiCo_2O_4$-CNT@DNA electrode capacitance. It was concluded that the interaction between CNTs and $NiCo_2O_4$ led to a greater specific capacitance of 760 F/g.

Nawwar et al. [59] fabricated Fe_3O_4-decorated CNTs (M-CNTs) for supercapacitor electrodes, which revealed capable functioning in a voltage window of 1.6 V. The M-CNT electrodes showed a great areal capacitance of 5.82 F cm^{-2} at different scan rates. In another approach, the electrochemical performance of $CuCo_2S_4$/CNT composite was explored in the energy storage processes [60]. The aggregation of $CuCo_2S_4$ nanocrystals could be prevented in the presence of CNTs. This is extremely favorable for specific redox reactions, especially relating to energy storage in supercapacitors. Furthermore, the specific capacitance can be increased at higher loadings of CNTs up to 3.2% due to electron transfer and the diffusion of electrolyte ions (Figure 11). The larger slope of the inclined line for the $CuCo_2S_4$/CNT electrode means lower ion diffusion resistance, which is favorable for faradaic redox reactions.

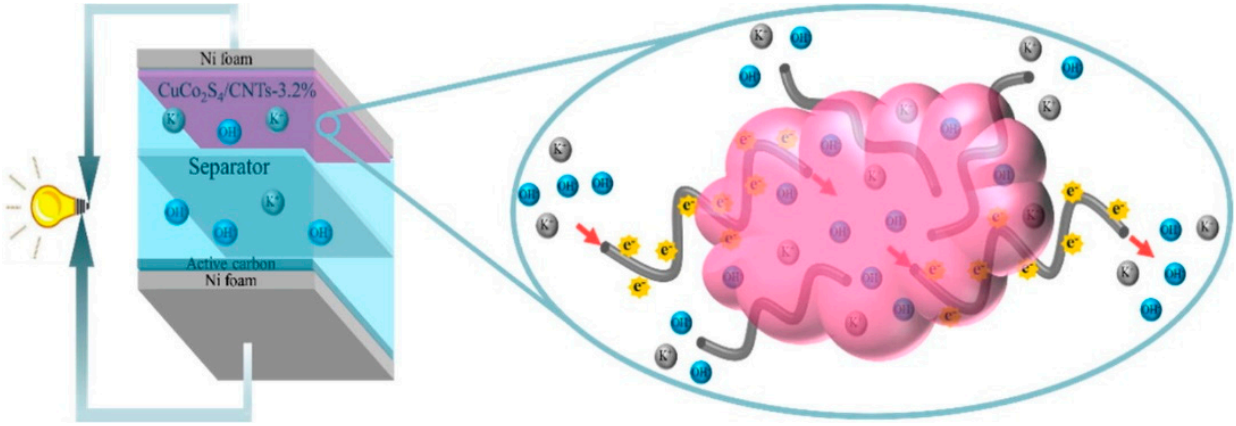


Figure 11. $CuCo_2S_4$/CNT-3.2% electrode with low series resistance and charge transfer resistance. Reproduced with permission [60].

Rostamabadi and Heydari-Bafrooei [61] studied a composite consisting of reduced graphene oxide (GO) and SWCNTs as the electrochemical probe. They observed the GO-SWCNT modified electrode only responds to the human epidermal growth factor receptor 2 (HER_2) and not to other proteins. It was concluded that the charge transfer resistance (R_{ct}) in electrochemical impedance spectroscopy (EIS) measurements increased with a rise in HER_2 concentration. Electrochemical capacitors, due to their fast-charging ability and stable cycling life span, have been widely used to develop novel electrode materials. According to Xue et al. [62], polymeric/inorganic nanohybrid-modified electrodes consisting of MWCNTs demonstrated a substantial specific capacitance of 6.5 mF cm^{-2}.

Due to their remarkable elastic and tensile strength, the development of CNT-reinforced polymer composites can contribute to a wide range of applications (Nurazzi et al. [63]. Sang et al. [64] investigated the effects of CNT morphology on the features of polymer composite properties. They concluded that thermoplastic polyurethane (TPU)/CNT and TPU/carbon nanostructure (CNS) composites can be exploited for strain sensor applications for the detection of human body motions. Some applications of CNT-reinforced polymer composites are summarized in Table 6.

Table 6. Literature survey of polymer composites reinforced with CNTs.

Applications	Preparation Method	CNTs Type and Dimensions	Remarks	Reference
Effects of CNTs on rubber-based composites in terms of mechanical properties	Rubber nanocomposites were prepared through the solution casting method	The CNT diameter was 15–17 nm	The mechanical performance of the nanocomposite shows filler-induced stiffness in the composite	[65]
Woven fabric composites reinforced with CNTs used in the automotive industry	Homogenization techniques for the fabrication of CNT-enriched polymer matrix	Randomly oriented CNTs	CNT-enriched polymer matrix improved mechanical properties such as Young's modulus	[66]
Fabrication of high-density polyethylene (HDPE)/carbon fiber (CF) composites reinforced with CNTs	Spray coating and the injection molding processes	Commercial MWCNTs prepared with the CVD technique with an average diameter of 20 nm	The tensile strength and modulus increased with the introduction of CNT due to the stronger adhesion at the interphase of CF and matrix	[67]
Polylactic acid-based composites reinforced with graphene and MWCNTs	Monofiller nanocomposites were prepared through melt extrusion	MWCNTs having purity > 95 wt% and diameter > 50 nm	Carbon nanofillers improve the hardness and elasticity of the nanocomposites	[68]
Dielectric composite reinforced with CNTs	In situ growth of CNTs using CVD	MWCNTs with outer diameters of 10–50 nm and lengths of several micrometers	The fabricated boron nitride nanosheets (BNNS)/CNT showed a high electrical resistivity of more than 1 Mohm-cm	[69]

4.2. Applications of CNTs as Catalyst Support

The application of CNTs as catalyst support has attracted considerable interest due to CNTs' resistance to acid or base environments and their high thermal stability. Chernyak et al. [70] used a cobalt-based CNT-supported catalyst in Fischer–Tropsch synthesis to study the effects of support functionalization on the catalytic activity. The results showed that highly oxidized CNTs improved Co dispersion and enhanced the catalytic activity.

Yahyazadeh et al. [71] reported that iron catalyst-supported CNTs showed high intrinsic activity compared with reference catalysts (Fe/Al_2O_3) in the FTS process. Additionally, the defects on the CNT surface resulting from the acid treatment increased the catalytic performance due to the low aggregation of Fe particles. Wu et al. [72] studied the hydrogenolysis of glycerol to 1,2-propanediol using a Cu-Ru/CNT catalyst. The dispersion of Cu-Ru particles on the external surface of MWCNTs resulted in a higher 1,2-propanediol selectivity compared to the selectivity obtained when Ru and Cu catalysts were used separately. Some applications of CNTs as the catalyst support for different chemical reactions are summarized in Table 7.

Table 7. Literature survey of the application of CNTs as a catalyst support.

Reaction	Catalyst	Operating Conditions	Remarks	Reference
Oxygen reduction reaction (ORR)	Nitrogen-doped CNTs supported Pt catalyst	4 mg of catalyst material/2 mL of ethanol and deionized water	Functionalized CNTs improve the deposition of Pt nanoparticles and offer superior performance as an ORR electrocatalyst	[73]
Methanol oxidation reaction	Sulfur-doped CNTs supported Pt catalyst	Reaction at 90 °C for 24 h	The electrochemical characterization of the catalysts suggests the oxidation of carbonaceous intermediates formed in the anodic scan	[74]
CO_2 methanation	CNTs supported mesoporous Ni catalyst	The catalytic performance was conducted in the temperature range from 200 to 400 °C under atmospheric pressure	CNTs supported the catalyst and showed high catalytic activities due to more lattice defects	[75]

Table 7. *Cont.*

Reaction	Catalyst	Operating Conditions	Remarks	Reference
Methanol oxidation reaction (MOR)	PtRu catalyst supported on thiol-functionalized CNTs (SH-CNTs)	The PtRu/CNTs working electrode was placed inside 0.5 M H_2SO_4 and methanol solution	PtRu/SH-CNT catalyst has enhanced catalytic activity for the MOR due to the electrooxidation of CO	[76]
Cross-coupling reactions	Palladium nanoparticles deposited on MWCNT (MWCNT/PdNP)	The Suzuki-Miyaura cross-coupling reaction for the synthesis of natural products and pharmaceuticals	MWCNT/PdNP showed excellent catalytic performance due to the curvature and polarizability of carbon nanostructures	[77]
Reduction of NO by CO in the presence of O_2	Cu-Ce catalysts supported on MWCNTs	Catalytic performance was evaluated using 200 mg of catalyst at different temperatures, from 140 to 260 °C	Cu:Ce/CNT catalyst revealed that an increased amount of Ce can adsorb and dissociate NO at low temperatures	[78]

4.3. Water Absorption and Filtration

CNTs can be used as the sorbent material in the control of water contamination that may arise from accidental leaking during transportation. Lico et al. [79] employed MWCNTs for the adsorption of unleaded gasoline from water due to their hollow and layered structures. It was found that unleaded gasoline accelerated the oxidation of MWCNTs, suggesting the use of small amounts of carbon nanomaterial to maximize the efficiency of the process. Moreover, CNT-based photothermal nanocomposite foam has been used for purification of water through a solar steam generation system [80]. Owing to the superior absorbance of CNTs in the solar spectrum, the resulting Fe_2O_3/CNT/Ni nanocomposite exhibited remarkable efficiency for solar-thermal energy conversion that enabled effective purification of water. In recent years, heavy metal removal using MWCNT-assisted membranes was reported by researchers [81]. It was found that increasing the MWCNTs' wt% in the polymer matrix can impact the pore sizes and enhance pure water flux. Pure CNT-based membrane adsorbents should present excellent recyclability to optimize the membrane selectivity and permeability.

Barrejón et al. [82] reported that the cross-linked CNT adsorbents demonstrate capable recyclability for the removal of organic pollutants from wastewater. Furthermore, cross-linked CNT adsorbents, due to their hydrophobic/superoleophilic surfaces, allow the diffusion of oils and nano droplets of water. Egbosiuba et al. [83] stated the adsorption capacity of functionalized MWCNTs for the abstraction of As(V) and Mn(VII) ions from wastewater. They observed that functionalized-MWCNT adsorbents showed strong electrostatic attraction towards heavy metals due to the enormous adsorption sites and with an increase in the temperature of the extraction medium. However, the adsorption capacity of MWCNTs was dependent on the pH. Table 8 lists a summary of different pollutant removal methods from wastewater using CNTs.

Table 8. Summary of different pollutants and CNTs' applications in water purification.

Chemical Types	Removal Approaches	Description	Reference
Humic acid	Facile vacuum-assisted filtration process	The separation performance of the nanofiltration membrane confirmed that the CNT content should be moderate to ensure dispersion and permeability.	[84]
Arsenic	Microwave-accelerated reaction system	The MWCNT-ZrO_2 sorbent has the advantage of effective arsenic removal over a wide range of pH.	[85]
Volatile organic materials	The phase inversion technique	Polysulfone/MWCNTs' membrane pore size and porosity start decreasing upon increasing MWCNTs' loading.	[86]

Table 8. *Cont.*

Chemical Types	Removal Approaches	Description	Reference
Sb(III)	Electrosorption–hydrothermal process	TiO_2-CNT filter shows the highest Sb(III) sorption capacity at a pH of 3.	[87]
Oily wastewater	The phase inversion method was employed for the preparation of polyethersulfone (PES) membranes.	The amino-functionalized MWCNTs onto the PES membrane showed an enhanced flux compared to the unmodified PES membrane.	[88]
Electromagnetic pollution	Pyrolysis and aqueous self-assembly methods used to prepare Co/ZnO/C@MWCNTs composites.	The addition of MWCNTs facilitates interfacial polarization and the conduction of electromagnetic waves, which results in the design of synthetic multi-component absorbers.	[89]

4.4. Gas Filtration and Sensor

Mukhtar et al. [90] showed the selective uptake of CO_2/CH_4 using functionalized MWCNTs at low pressures. They concluded that highly selective separation of CO_2 and CH_4 was due to the cooperative forces between CO_2 molecules and oxygen-based functionalities in MWCNTs. Moreover, the impact of temperature on CO_2 adsorption capacity confirmed that the adsorption is exothermic and thermodynamically controlled. Figure 12 shows oxygen-rich surface functional groups coated on MWCNTs after mixing of raw-MWCNTs with H_2SO_4 and nitric acid.

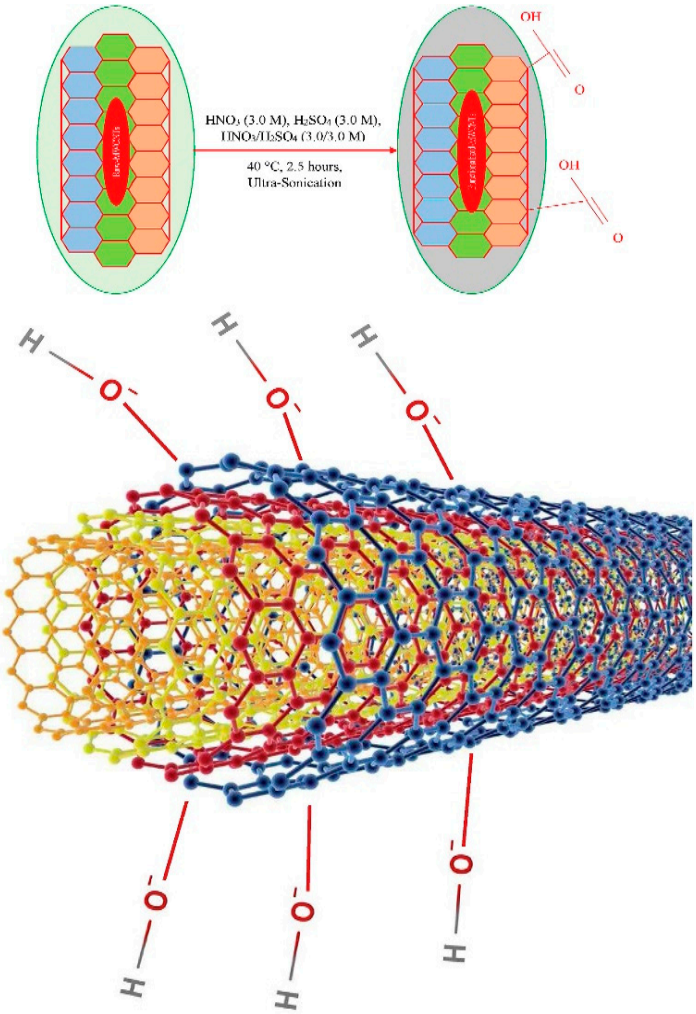


Figure 12. Attachment of oxygen-based functional groups onto MWCNTs. Reproduced with permission [90].

Considering gas-sensing applications, Seekaew et al. [91] fabricated TiO_2 nanoparticle-decorated three-dimensional graphene CNT nanostructures (3D TiO_2/G-CNT) to assess the toluene gas response. The results showed satisfactory reproducibility for toluene detection at room temperatures and improvement in the gas response with increasing Ti loading. Moreover, 3D TiO_2/G-CNT sensors also confirmed the p-type gas-sensing activities at a concentration of 50–500 ppm. Sacco et al. [92] studied NO_2 gas sensors based on SWCNTs for detecting low NO_2 concentrations at room temperatures. The results showed that the sensing occurred at the interface of the metal electrode and SWCNT due to changes in the Schottky barriers. Jeon et al. [93] studied the sensing performance of NO using random networks of a functionalized SWCNT. Selectivity of the SWCNT-based NO sensor enabled the detection of NO_2 gas at 100 ppb under ambient conditions. As shown in Figure 13, Yang et al. [94] proposed $NiWO_4$ decorated with MWCNTs for high-performance NH_3 detection. The sensitivity of the gas sensor shows an excellent performance because of the high surface area and introduction of specific amounts of MWCNTs. Additionally, the prepared $NiWO_4$/MWCNT sensors increased the active sites to furnish a superior channel for the electron transport. A large number of p-n heterojunctions are formed at a MWCNT's surface, and they change its electron density due to the fact that conversion of O_2 to O^{2-} depends on temperature.

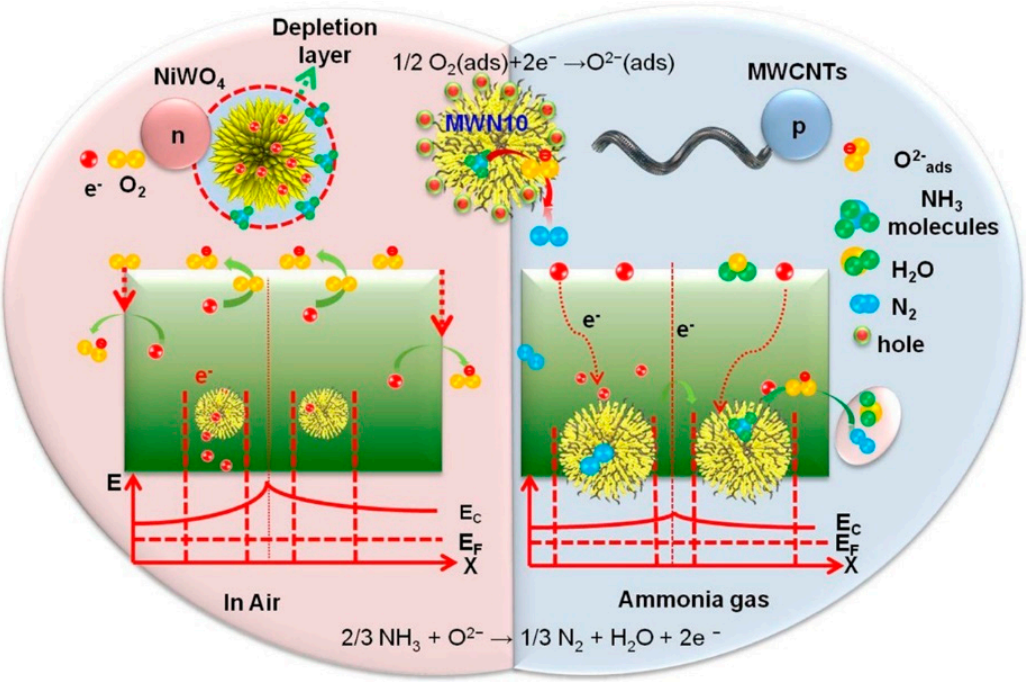


Figure 13. Representation of the gas-sensing mechanism of $NiWO_4$/MWCNT. Reproduced with permission [94].

Kaviyarasu et al. [95] explored the ZnO-doped SWCNT nanostructures for the opto-electronic properties and sensing properties of ethanol gas. ZnO/SWCNT nanocrystalline thin film showed high reactivity toward gases at temperatures up to 170 °C. An increase in the ethanol concentration from 100 ppm to 500 ppm improved gas sensitivity because of the charge transfer.

4.5. Application of CNT-based Composite Membranes

To provide a better overview of application of CNTs, the following section demonstrates the feasibility of CNT-based membranes. A particular advantage of CNTs is discriminating between particles that have a size on the Å scale and repeated use with full filtering efficiency. There are two types of CNT-based membranes including vertically aligned carbon nanotube (VA-CNT) and mixed-matrix CNT membranes. CNT membranes in water

purification can be used as a substitute for traditional ultrafiltration (UF) membranes. A recent study carried out by Ma et al. reviews the fabrication methods for CNT-based composite membranes in detail. It was reported that functionalization of CNTs is a key pre-step for synthesis of CNT-based composite membranes [96]. In another study, the electrochemically active CNT membrane was investigated for desalination and purification of water [97]. Electrochemically active CNT membrane filters decrease the fouling of filtration medium through biological inactivation. It has been revealed that surface modification of CNTs through covalent functionalization makes CNTs soluble in many organic solvents. Incorporation with metal leads to better CNT performance as a photo-catalyst and helps in the reduction of adsorbed oxygen to form superoxide anion radicals. Increasing the amount of MWCNTs can forbid the microorganisms' development. However, formation of bubbles blocks the pores of CNTs and may limit the overall water flux.

CNTs have gained considerable recent attention due to their application as both electrode and filtration media. The CNT networks are stable, and this indicates the electron-transfer can be enhanced by tailoring the CNT surface. Furthermore, the excellent performance at a neutral pH can be attributed to electrokinetic processes such as electrophoresis and dielectrophoresis approaches [98]. In principle, applications of membrane technology are common at removing colloidal and particulate pollutants. Electrically conducting membranes (EMs) are prepared by depositing a thin layer of CNTs on a relatively hydrophilic support. Furthermore, low-pressure EMs for water reuse are fabricated using thin-film coatings of CNTs and offer outstanding potential in terms of minimizing membrane pre-treatment costs [99].

The problem arises of synthesizing CNTs at an effective cost and producing non-defective structures. CNTs act as an excellent adsorbent, biosensor, and energy transfer material [100]. The mechanism of the formation of CNTs under microwave radiation is required to underpin science. The optimization of CNTs' properties and the ability to control the morphology can lead to superior properties. Furthermore, the synthesis of CNTs using biomass without structure defects limits their application and large-scale production [101].

5. Conclusions

CNTs show many extreme properties in comparison to any other known material such as amazing electronic and mechanical properties. Large-scale production of high-quality CNTs is important to develop cost-effective and reliable approaches such as the CCVD process. The CCVD technique acquired more research attention owing to low-temperature synthesis, simplicity in operation, and energy efficiency. Furthermore, CNTs have made great breakthroughs in composites, sensors, and electrochemical device applications due to their high electric activity and fast electron transfer. The surface modifications of CNTs can enhance the mechanical, thermal, and electrical characteristics due to interactions between the CNTs and matrix. A wide range of analytical techniques provide the information needed for particular properties of CNTs.

Funding: The authors would like to thank the Natural Sciences and Engineering Research Council of Canada (NSERC) and the Canada Research Chair (CRC) program for funding this study.

Conflicts of Interest: The authors declare no conflict of interest.

Abbreviations

AFM	Atomic-force microscopy
BNNS	Boron nitride nanosheets
CF	Carbon fiber
CNS	Carbon nanostructure
CNTs	Carbon nanotubes
CCVD	Catalytic chemical vapor deposition
Rct	Charge transfer resistance

CVD	Chemical vapor deposition
DWCNTs	Double-walled carbon nanotubes
EIS	Electrochemical impedance spectroscopy
FT-IR	Fourier transform infrared spectroscopy
GO	Graphene oxide
HDPE	High-density polyethylene
HRTEM	High-resolution transmission electron microscopy
HER2	Human epidermal growth factor receptor 2
MOR	Methanol oxidation reaction
MWCNTs	Multi-walled carbon nanotubes
ORR	Oxygen reduction reaction
PES	Polyethersulfone
SWCNTs	Single-walled carbon nanotubes
TPU	Thermoplastic polyurethane
SH-CNTs	Thiol-functionalized carbon nanotubes
TGA	Thermogravimetric analysis
TEM	Transmission electron microscopy
XRD	X-ray diffraction
XPS	X-ray photoelectron spectroscopy

References

1. Jia, X.; Wei, F. Advances in Production and Applications of Carbon Nanotubes. *Top. Curr. Chem. (Cham)* **2017**, *375*, 18. [CrossRef] [PubMed]
2. Panchal, M.B.; Upadhyay, S.H. Cantilevered Single Walled Boron Nitride Nanotube Based Nanomechanical Resonators of Zigzag and Armchair Forms. Phys. E Low-dimensional Syst. *Nanostructures* **2013**, *50*, 73–82. [CrossRef]
3. Cho, T.H.; Su, W.S.; Leung, T.C.; Ren, W.; Chan, C.T. Electronic and Optical Properties of Single-Walled Carbon Nanotubes under a Uniform Transverse Electric Field: A First-Principles Study. *Phys. Rev. B* **2009**, *79*, 235123. [CrossRef]
4. Zaporotskova, I.V.; Boroznina, N.P.; Parkhomenko, Y.N.; Kozhitov, L. V Carbon Nanotubes: Sensor Properties. A Review. *Mod. Electron. Mater.* **2016**, *2*, 95–105. [CrossRef]
5. Singh, Y.T.; Patra, P.K.; Hieu, N.N.; Rai, D.P. Study of Electronic and Mechanical Properties of Single Walled Carbon Nanotube (SWCNT) via Substitutional Boron Doping in Zigzag and Armchair Pattern. *Surf. Interfaces* **2022**, *29*, 101815. [CrossRef]
6. Zhang, J.; Tahmasebi, A.; Omoriyekomwan, J.E.; Yu, J. Production of Carbon Nanotubes on Bio-Char at Low Temperature via Microwave-Assisted CVD Using Ni Catalyst. *Diam. Relat. Mater.* **2019**, *91*, 98–106. [CrossRef]
7. Murjani, B.O.; Kadu, P.S.; Bansod, M.; Vaidya, S.S.; Yadav, M.D. Carbon Nanotubes in Biomedical Applications: Current Status, Promises, and Challenges. *Carbon Lett.* **2022**, *32*, 1207–1226. [CrossRef]
8. Maheswaran, R.; Shanmugavel, B.P. A Critical Review of the Role of Carbon Nanotubes in the Progress of Next-Generation Electronic Applications. *J. Electron. Mater.* **2022**, *51*, 2786–2800. [CrossRef]
9. Yahyazadeh, A.; Khoshandam, B. Carbon Nanotube Synthesis via the Catalytic Chemical Vapor Deposition of Methane in the Presence of Iron, Molybdenum, and Iron–Molybdenum Alloy Thin Layer Catalysts. *Results Phys.* **2017**, *7*, 3826–3837. [CrossRef]
10. Rahman, G.; Najaf, Z.; Mehmood, A.; Bilal, S.; Shah, A.u.H.A.; Mian, S.A.; Ali, G. An Overview of the Recent Progress in the Synthesis and Applications of Carbon Nanotubes. *C* **2019**, *5*, 3. [CrossRef]
11. Maria, K.H.; Mieno, T. Synthesis of Single-Walled Carbon Nanotubes by Low-Frequency Bipolar Pulsed Arc Discharge Method. *Vacuum* **2015**, *113*, 11–18. [CrossRef]
12. Raniszewski, G.; Wiak, S.; Pietrzak, L.; Szymanski, L.; Kolacinski, Z. Influence of Plasma Jet Temperature Profiles in Arc Discharge Methods of Carbon Nanotubes Synthesis. *Nanomaterials* **2017**, *7*, 50. [CrossRef] [PubMed]
13. Bagiante, S.; Scalese, S.; Scuderi, V.; D'Urso, L.; Messina, E.; Compagnini, G.; Privitera, V. Role of the Growth Parameters on the Structural Order of MWCNTs Produced by Arc Discharge in Liquid Nitrogen. *Phys. Status Solidi* **2010**, *247*, 884–887. [CrossRef]
14. Arora, N.; Sharma, N.N. Arc Discharge Synthesis of Carbon Nanotubes: Comprehensive Review. *Diam. Relat. Mater.* **2014**, *50*, 135–150. [CrossRef]
15. Awadallah, A.E.; Abdel-Hamid, S.M.; El-Desouki, D.S.; Aboul-Enein, A.A.; Aboul-Gheit, A.K. Synthesis of Carbon Nanotubes by CCVD of Natural Gas Using Hydrotreating Catalysts. *Egypt. J. Pet.* **2012**, *21*, 101–107. [CrossRef]
16. Gohier, A.; Ewels, C.P.; Minea, T.M.; Djouadi, M.A. Carbon Nanotube Growth Mechanism Switches from Tip- to Base-Growth with Decreasing Catalyst Particle Size. *Carbon N. Y.* **2008**, *46*, 1331–1338. [CrossRef]
17. Dijon, J.; Szkutnik, P.D.; Fournier, A.; Goislard de Monsabert, T.; Okuno, H.; Quesnel, E.; Muffato, V.; De Vito, E.; Bendiab, N.; Bogner, A.; et al. How to Switch from a Tip to Base Growth Mechanism in Carbon Nanotube Growth by Catalytic Chemical Vapour Deposition. *Carbon N. Y.* **2010**, *48*, 3953–3963. [CrossRef]
18. Yan, Y.; Miao, J.; Yang, Z.; Xiao, F.-X.; Yang, H.; Liu, B.; Yang, Y. Carbon Nanotube Catalysts: Recent Advances in Synthesis, Characterization and Applications. *Chem. Soc. Rev.* **2015**, *44*, 3295–3346. [CrossRef]

19. Rattanaamonkulchai, R.; Kludpantanapan, T.; Srifa, A.; Koo-Amornpattana, W.; Chaiwat, W.; Sakdaronnarong, C.; Charinpanitkul, T.; Assabumrungrat, S.; Wongsakulphasatch, S.; Show, P.-L.; et al. Simultaneous Production of Hydrogen and Carbon Nanotubes from Biogas over Mono- and Bimetallic Catalyst. *J. Environ. Chem. Eng.* **2022**, *10*, 107910. [CrossRef]
20. Bankole, M.T.; Mohammed, I.A.; Abdulkareem, A.S.; Tijani, J.O.; Ochigbo, S.S.; Abubakre, O.K.; Afolabi, A.S. Optimization of Supported Bimetallic (Fe-Co/$CaCO_3$) Catalyst Synthesis Parameters for Carbon Nanotubes Growth Using Factorial Experimental Design. *J. Alloys Compd.* **2018**, *749*, 85–102. [CrossRef]
21. Fedorovskaya, E.O.; Bulusheva, L.G.; Kurenya, A.G.; Asanov, I.P.; Rudina, N.A.; Funtov, K.O.; Lyubutin, I.S.; Okotrub, A. V Supercapacitor Performance of Vertically Aligned Multiwall Carbon Nanotubes Produced by Aerosol-Assisted CCVD Method. *Electrochim. Acta* **2014**, *139*, 165–172. [CrossRef]
22. Sharifi, T.; Nitze, F.; Barzegar, H.R.; Tai, C.-W.; Mazurkiewicz, M.; Malolepszy, A.; Stobinski, L.; Wågberg, T. Nitrogen Doped Multi Walled Carbon Nanotubes Produced by CVD-Correlating XPS and Raman Spectroscopy for the Study of Nitrogen Inclusion. *Carbon N. Y.* **2012**, *50*, 3535–3541. [CrossRef]
23. Toussi, S.M.; Fakhru'L-Razi, A.; Luqman Chuah, A.; Suraya, A.R. Optimization of Synthesis Condition for Carbon Nanotubes by Catalytic Chemical Vapor Deposition (CCVD). *IOP Conf. Ser. Mater. Sci. Eng.* **2011**, *17*, 012003. [CrossRef]
24. Pasha, M.A.; Shafiekhani, A.; Vesaghi, M.A. Hot Filament CVD of Fe–Cr Catalyst for Thermal CVD Carbon Nanotube Growth from Liquid Petroleum Gas. *Appl. Surf. Sci.* **2009**, *256*, 1365–1371. [CrossRef]
25. Dhore, V.G.; Rathod, W.S.; Patil, K.N. Synthesis and Characterization of High Yield Multiwalled Carbon Nanotubes by Ternary Catalyst. *Mater. Today Proc.* **2018**, *5*, 3432–3437. [CrossRef]
26. Szabó, A.; Kecsenovity, E.; Pápa, Z.; Gyulavári, T.; Németh, K.; Horvath, E.; Hernadi, K. Influence of Synthesis Parameters on CCVD Growth of Vertically Aligned Carbon Nanotubes over Aluminum Substrate. *Sci. Rep.* **2017**, *7*, 9557. [CrossRef]
27. Zhang, M.; Yudasaka, M.; Iijima, S. Production of Large-Diameter Single-Wall Carbon Nanotubes by Adding Fe to a NiCo Catalyst in Laser Ablation. *J. Phys. Chem. B* **2004**, *108*, 12757–12762. [CrossRef]
28. Zhang, H.; Ding, Y.; Wu, C.; Chen, Y.; Zhu, Y.; He, Y.; Zhong, S. The Effect of Laser Power on the Formation of Carbon Nanotubes Prepared in CO_2 Continuous Wave Laser Ablation at Room Temperature. *Phys. B Condens. Matter* **2003**, *325*, 224–229. [CrossRef]
29. Bota, P.M.; Dorobantu, D.; Boerasu, I.; Bojin, D.; Enachescu, M. New Laser Ablation Chamber for Producing Carbon Nanomaterials Using Excimer Laser. *Mater. Res. Innov.* **2015**, *19*, 33–39. [CrossRef]
30. Yuge, R.; Toyama, K.; Ichihashi, T.; Ohkawa, T.; Aoki, Y.; Manako, T. Characterization and Field Emission Properties of Multi-Walled Carbon Nanotubes with Fine Crystallinity Prepared by CO_2 Laser Ablation. *Appl. Surf. Sci.* **2012**, *258*, 6958–6962. [CrossRef]
31. Hameed, R.; Khashan, K.S.; Sulaiman, G.M. Preparation and Characterization of Graphene Sheet Prepared by Laser Ablation in Liquid. *Mater. Today Proc.* **2020**, *20*, 535–539. [CrossRef]
32. Tabatabaie, N.; Dorranian, D. Effect of Fluence on Carbon Nanostructures Produced by Laser Ablation in Liquid Nitrogen. *Appl. Phys. A* **2016**, *122*, 558. [CrossRef]
33. Mwafy, E.A.; Mostafa, A.M. Efficient Removal of Cu (II) by SnO_2/MWCNTs Nanocomposite by Pulsed Laser Ablation Method. *Nano-Struct. Nano-Objects* **2020**, *24*, 100591. [CrossRef]
34. Szabó, A.; Perri, C.; Csató, A.; Giordano, G.; Vuono, D.; Nagy, J.B. Synthesis Methods of Carbon Nanotubes and Related Materials. *Materials* **2010**, *3*, 3092–3140. [CrossRef]
35. Teimuri-Mofrad, R.; Hadi, R.; Abbasi, H.; Fadakar Bajeh Baj, R. Synthesis, Characterization and Electrochemical Study of Carbon Nanotube/Chitosan-Ferrocene Nanocomposite Electrode as Supercapacitor Material. *J. Electron. Mater.* **2019**, *48*, 4573–4581. [CrossRef]
36. Basiuk, E.V.; Huerta, L.; Basiuk, V.A. Noncovalent Bonding of 3d Metal(II) Phthalocyanines with Single-Walled Carbon Nanotubes: A Combined DFT and XPS Study. *Appl. Surf. Sci.* **2019**, *470*, 622–630. [CrossRef]
37. Saravanakkumar, D.; Oualid, H.A.; Brahmi, Y.; Ayeshamariam, A.; Karunanaithy, M.; Saleem, A.M.; Kaviyarasu, K.; Sivaranjani, S.; Jayachandran, M. Synthesis and Characterization of CuO/ZnO/CNTs Thin Films on Copper Substrate and Its Photocatalytic Applications. *OpenNano* **2019**, *4*, 100025. [CrossRef]
38. Li, Z.; Deng, L.; Kinloch, I.A.; Young, R.J. Raman Spectroscopy of Carbon Materials and Their Composites: Graphene, Nanotubes and Fibres. *Prog. Mater. Sci.* **2023**, *135*, 101089. [CrossRef]
39. Affonso, L.N.; Marques, J.L.; Lima, V.V.C.; Gonçalves, J.O.; Barbosa, S.C.; Primel, E.G.; Burgo, T.A.L.; Dotto, G.L.; Pinto, L.A.A.; Cadaval, T.R.S. Removal of Fluoride from Fertilizer Industry Effluent Using Carbon Nanotubes Stabilized in Chitosan Sponge. *J. Hazard. Mater.* **2020**, *388*, 122042. [CrossRef]
40. Parmar, K.R.; Dora, D.T.K.; Pant, K.K.; Roy, S. An Ultra-Light Flexible Aerogel-Based on Methane Derived CNTs as a Reinforcing Agent in Silica-CMC Matrix for Efficient Oil Adsorption. *J. Hazard. Mater.* **2019**, *375*, 206–215. [CrossRef]
41. Dong, B.; Li, S.; Zhang, X.; Wang, J.; Peng, H. Synthesis and Characterization of Nanoalumina and CNTs-Reinforced Microcapsules with n-Dodecane as a Phase Change Material for Cold Energy Storage. *Energy Fuels* **2020**, *34*, 7700–7708. [CrossRef]
42. Twinkle; Kaur, M.; Gowsamy, J.K.; Kumar, P.; Kumar, S. Synthesis and Characterization of CNT/PVDF Paper for Electronic and Energy Storage Applications. *Emergent Mater.* **2020**, *3*, 181–185. [CrossRef]
43. Hoyos-Palacio, L.M.; Cuesta Castro, D.P.; Ortiz-Trujillo, I.C.; Botero Palacio, L.E.; Galeano Upegui, B.J.; Escobar Mora, N.J.; Carlos Cornelio, J.A. Compounds of Carbon Nanotubes Decorated with Silver Nanoparticles via In-Situ by Chemical Vapor Deposition (CVD). *J. Mater. Res. Technol.* **2019**, *8*, 5893–5898. [CrossRef]

44. Peretz, S.; Regev, O. Carbon Nanotubes as Nanocarriers in Medicine. *Curr. Opin. Colloid Interface Sci.* **2012**, *17*, 360–368. [CrossRef]
45. Gomez-Gualdron, D.A.; Burgos, J.C.; Yu, J.; Balbuena, P.B. Carbon Nanotubes: Engineering Biomedical Applications. *Prog. Mol. Biol. Transl. Sci.* **2011**, *104*, 175–245.
46. Wang, L.; Xie, S.; Wang, Z.; Liu, F.; Yang, Y.; Tang, C.; Wu, X.; Liu, P.; Li, Y.; Saiyin, H.; et al. Functionalized Helical Fibre Bundles of Carbon Nanotubes as Electrochemical Sensors for Long-Term in Vivo Monitoring of Multiple Disease Biomarkers. *Nat. Biomed. Eng.* **2020**, *4*, 159–171. [CrossRef] [PubMed]
47. Park, S.; Park, J.; Jo, I.; Cho, S.-P.; Sung, D.; Ryu, S.; Park, M.; Min, K.-A.; Kim, J.; Hong, S.; et al. In Situ Hybridization of Carbon Nanotubes with Bacterial Cellulose for Three-Dimensional Hybrid Bioscaffolds. *Biomaterials* **2015**, *58*, 93–102. [CrossRef] [PubMed]
48. Chen, Z.; Wu, Y.; Yang, Y.; Li, J.; Xie, B.; Li, X.; Lei, S.; Ou-Yang, J.; Yang, X.; Zhou, Q.; et al. Multilayered Carbon Nanotube Yarn Based Optoacoustic Transducer with High Energy Conversion Efficiency for Ultrasound Application. *Nano Energy* **2018**, *46*, 314–321. [CrossRef]
49. Patlolla, A.K.; Patra, P.K.; Flountan, M.; Tchounwou, P.B. Cytogenetic Evaluation of Functionalized Single-walled Carbon Nanotube in Mice Bone Marrow Cells. *Environ. Toxicol.* **2016**, *31*, 1091–1102. [CrossRef]
50. Lu, X.; Zhu, Y.; Bai, R.; Wu, Z.; Qian, W.; Yang, L.; Cai, R.; Yan, H.; Li, T.; Pandey, V. Long-Term Pulmonary Exposure to Multi-Walled Carbon Nanotubes Promotes Breast Cancer Metastatic Cascades. *Nat. Nanotechnol.* **2019**, *14*, 719–727. [CrossRef]
51. Zakaria, A.B.; Picaud, F.; Rattier, T.; Pudlo, M.; Saviot, L.; Chassagnon, R.; Lherminier, J.; Gharbi, T.; Micheau, O.; Herlem, G. Nanovectorization of TRAIL with Single Wall Carbon Nanotubes Enhances Tumor Cell Killing. *Nano Lett.* **2015**, *15*, 891–895. [CrossRef] [PubMed]
52. Tohidlou, H.; Shafiei, S.S.; Abbasi, S.; Asadi-Eydivand, M.; Fathi-Roudsari, M. Amine-Functionalized Single-Walled Carbon Nanotube/Polycaprolactone Electrospun Scaffold for Bone Tissue Engineering: In Vitro Study. *Fibers Polym.* **2019**, *20*, 1869–1882. [CrossRef]
53. Ramachandran, K.; Raj Kumar, T.; Babu, K.J.; Gnana Kumar, G. Ni-Co Bimetal Nanowires Filled Multiwalled Carbon Nanotubes for the Highly Sensitive and Selective Non-Enzymatic Glucose Sensor Applications. *Sci. Rep.* **2016**, *6*, 36583. [CrossRef]
54. Lai, Y.-T.; Kuo, J.-C.; Yang, Y.-J. A Novel Gas Sensor Using Polymer-Dispersed Liquid Crystal Doped with Carbon Nanotubes. *Sens. Actuators A Phys.* **2014**, *215*, 83–88. [CrossRef]
55. Khani, H.; Rofouei, M.K.; Arab, P.; Gupta, V.K.; Vafaei, Z. Multi-Walled Carbon Nanotubes-Ionic Liquid-Carbon Paste Electrode as a Super Selectivity Sensor: Application to Potentiometric Monitoring of Mercury Ion(II). *J. Hazard. Mater.* **2010**, *183*, 402–409. [CrossRef]
56. Wu, H.-X.; Cao, W.-M.; Li, Y.; Liu, G.; Wen, Y.; Yang, H.-F.; Yang, S.-P. In Situ Growth of Copper Nanoparticles on Multiwalled Carbon Nanotubes and Their Application as Non-Enzymatic Glucose Sensor Materials. *Electrochim. Acta* **2010**, *55*, 3734–3740. [CrossRef]
57. Tabassum, H.; Mahmood, A.; Zhu, B.; Liang, Z.; Zhong, R.; Guo, S.; Zou, R. Recent Advances in Confining Metal-Based Nanoparticles into Carbon Nanotubes for Electrochemical Energy Conversion and Storage Devices. *Energy Environ. Sci.* **2019**, *12*, 2924–2956. [CrossRef]
58. Xue, Y.; Chen, T.; Song, S.; Kim, P.; Bae, J. DNA-Directed Fabrication of $NiCo_2O_4$ Nanoparticles on Carbon Nanotubes as Electrodes for High-Performance Battery-like Electrochemical Capacitive Energy Storage Device. *Nano Energy* **2019**, *56*, 751–758. [CrossRef]
59. Nawwar, M.; Poon, R.; Chen, R.; Sahu, R.P.; Puri, I.K.; Zhitomirsky, I. High Areal Capacitance of Fe_3O_4-decorated Carbon Nanotubes for Supercapacitor Electrodes. *Carbon Energy* **2019**, *1*, 124–133. [CrossRef]
60. Li, H.; Li, Z.; Wu, Z.; Sun, M.; Han, S.; Cai, C.; Shen, W.; Liu, X.; Fu, Y. Enhanced Electrochemical Performance of $CuCo_2S_4$/Carbon Nanotubes Composite as Electrode Material for Supercapacitors. *J. Colloid Interface Sci.* **2019**, *549*, 105–113. [CrossRef]
61. Rostamabadi, P.F.; Heydari-Bafrooei, E. Impedimetric Aptasensing of the Breast Cancer Biomarker HER2 Using a Glassy Carbon Electrode Modified with Gold Nanoparticles in a Composite Consisting of Electrochemically Reduced Graphene Oxide and Single-Walled Carbon Nanotubes. *Microchim. Acta* **2019**, *186*, 495. [CrossRef]
62. Xue, T.; Liu, P.; Zhang, J.; Xu, J.; Zhang, G.; Zhou, P.; Li, Y.; Zhu, Y.; Lu, X.; Wen, Y. Multiwalled Carbon Nanotube-N-Doped Graphene/Poly(3,4-Ethylenedioxythiophene):Poly(Styrenesulfonate) Nanohybrid for Electrochemical Application in Intelligent Sensors and Supercapacitors. *ACS Omega* **2020**, *5*, 28452–28462. [CrossRef]
63. Mohd Nurazzi, N.; Asyraf, M.R.M.; Khalina, A.; Abdullah, N.; Sabaruddin, F.A.; Kamarudin, S.H.; Ahmad, S.; Mahat, A.M.; Lee, C.L.; Aisyah, H.A. Fabrication, Functionalization, and Application of Carbon Nanotube-Reinforced Polymer Composite: An Overview. *Polymers* **2021**, *13*, 1047. [CrossRef] [PubMed]
64. Sang, Z.; Ke, K.; Manas-Zloczower, I. Effect of Carbon Nanotube Morphology on Properties in Thermoplastic Elastomer Composites for Strain Sensors. *Compos. Part A Appl. Sci. Manuf.* **2019**, *121*, 207–212. [CrossRef]
65. Kumar, V.; Kumar, A.; Han, S.S.; Park, S.-S. RTV Silicone Rubber Composites Reinforced with Carbon Nanotubes, Titanium-Di-Oxide and Their Hybrid: Mechanical and Piezoelectric Actuation Performance. *Nano Mater. Sci.* **2021**, *3*, 233–240. [CrossRef]
66. Fantuzzi, N.; Bacciocchi, M.; Agnelli, J.; Benedetti, D. Three-Phase Homogenization Procedure for Woven Fabric Composites Reinforced by Carbon Nanotubes in Thermal Environment. *Compos. Struct.* **2020**, *254*, 112840. [CrossRef]
67. Hu, C.; Liao, X.; Qin, Q.-H.; Wang, G. The Fabrication and Characterization of High Density Polyethylene Composites Reinforced by Carbon Nanotube Coated Carbon Fibers. *Compos. Part A Appl. Sci. Manuf.* **2019**, *121*, 149–156. [CrossRef]

68. Batakliev, T.; Georgiev, V.; Ivanov, E.; Kotsilkova, R.; Di Maio, R.; Silvestre, C.; Cimmino, S. Nanoindentation Analysis of 3D Printed Poly (Lactic Acid)-based Composites Reinforced with Graphene and Multiwall Carbon Nanotubes. *J. Appl. Polym. Sci.* **2019**, *136*, 47260. [CrossRef]
69. Li, Y.; Tian, X.; Yang, W.; Li, Q.; Hou, L.; Zhu, Z.; Tang, Y.; Wang, M.; Zhang, B.; Pan, T.; et al. Dielectric Composite Reinforced by In-Situ Growth of Carbon Nanotubes on Boron Nitride Nanosheets with High Thermal Conductivity and Mechanical Strength. *Chem. Eng. J.* **2019**, *358*, 718–724. [CrossRef]
70. Chernyak, S.; Burtsev, A.; Maksimov, S.; Kupreenko, S.; Maslakov, K.; Savilov, S. Structural Evolution, Stability, Deactivation and Regeneration of Fischer-Tropsch Cobalt-Based Catalysts Supported on Carbon Nanotubes. *Appl. Catal. A Gen.* **2020**, *603*, 117741. [CrossRef]
71. Yahyazadeh, A.; Borugadda, V.B.; Dalai, A.K.; Zhang, L. Optimization of Carbon Nanotube Growth via Response Surface Methodology for Fischer-Tropsch Synthesis over Fe/CNT Catalyst. *Catal. Today* **2022**, *404*, 117–131. [CrossRef]
72. Wu, Z.; Mao, Y.; Wang, X.; Zhang, M. Preparation of a Cu–Ru/Carbon Nanotube Catalyst for Hydrogenolysis of Glycerol to 1,2-Propanediol via Hydrogen Spillover. *Green Chem.* **2011**, *13*, 1311–1316. [CrossRef]
73. Higgins, D.C.; Meza, D.; Chen, Z. Nitrogen-Doped Carbon Nanotubes as Platinum Catalyst Supports for Oxygen Reduction Reaction in Proton Exchange Membrane Fuel Cells. *J. Phys. Chem. C* **2010**, *114*, 21982–21988. [CrossRef]
74. Fan, J.-J.; Fan, Y.-J.; Wang, R.-X.; Xiang, S.; Tang, H.-G.; Sun, S.-G. A Novel Strategy for the Synthesis of Sulfur-Doped Carbon Nanotubes as a Highly Efficient Pt Catalyst Support toward the Methanol Oxidation Reaction. *J. Mater. Chem. A* **2017**, *5*, 19467–19475. [CrossRef]
75. Wang, W.; Chu, W.; Wang, N.; Yang, W.; Jiang, C. Mesoporous Nickel Catalyst Supported on Multi-Walled Carbon Nanotubes for Carbon Dioxide Methanation. *Int. J. Hydrogen Energy* **2016**, *41*, 967–975. [CrossRef]
76. Guo, L.; Chen, S.; Li, L.; Wei, Z. A CO-Tolerant PtRu Catalyst Supported on Thiol-Functionalized Carbon Nanotubes for the Methanol Oxidation Reaction. *J. Power Sources* **2014**, *247*, 360–364. [CrossRef]
77. Cornelio, B.; Rance, G.A.; Laronze-Cochard, M.; Fontana, A.; Sapi, J.; Khlobystov, A.N. Palladium Nanoparticles on Carbon Nanotubes as Catalysts of Cross-Coupling Reactions. *J. Mater. Chem. A* **2013**, *1*, 8737–8744. [CrossRef]
78. Gholami, Z.; Luo, G. Low-Temperature Selective Catalytic Reduction of NO by CO in the Presence of O2 over Cu:Ce Catalysts Supported by Multiwalled Carbon Nanotubes. *Ind. Eng. Chem. Res.* **2018**, *57*, 8871–8883. [CrossRef]
79. Lico, D.; Vuono, D.; Siciliano, C.; Nagy, J.B.; De Luca, P. Removal of Unleaded Gasoline from Water by Multi-Walled Carbon Nanotubes. *J. Environ. Manag.* **2019**, *237*, 636–643. [CrossRef]
80. Han, S.; Yang, J.; Li, X.; Li, W.; Zhang, X.; Koratkar, N.; Yu, Z.-Z. Flame Synthesis of Superhydrophilic Carbon Nanotubes/Ni Foam Decorated with Fe2O3 Nanoparticles for Water Purification via Solar Steam Generation. *ACS Appl. Mater. Interfaces* **2020**, *12*, 13229–13238. [CrossRef]
81. Chandrashekhar Nayak, M.; Isloor, A.M.; Inamuddin; Lakshmi, B.; Marwani, H.M.; Khan, I. Polyphenylsulfone/Multiwalled Carbon Nanotubes Mixed Ultrafiltration Membranes: Fabrication, Characterization and Removal of Heavy Metals Pb2+, Hg2+, and Cd2+ from Aqueous Solutions. *Arab. J. Chem.* **2020**, *13*, 4661–4672. [CrossRef]
82. Barrejón, M.; Syrgiannis, Z.; Burian, M.; Bosi, S.; Montini, T.; Fornasiero, P.; Amenitsch, H.; Prato, M. Cross-Linked Carbon Nanotube Adsorbents for Water Treatment: Tuning the Sorption Capacity through Chemical Functionalization. *ACS Appl. Mater. Interfaces* **2019**, *11*, 12920–12930. [CrossRef] [PubMed]
83. Egbosiuba, T.C.; Abdulkareem, A.S.; Kovo, A.S.; Afolabi, E.A.; Tijani, J.O.; Roos, W.D. Enhanced Adsorption of As(V) and Mn(VII) from Industrial Wastewater Using Multi-Walled Carbon Nanotubes and Carboxylated Multi-Walled Carbon Nanotubes. *Chemosphere* **2020**, *254*, 126780. [CrossRef] [PubMed]
84. Chen, X.; Qiu, M.; Ding, H.; Fu, K.; Fan, Y. A Reduced Graphene Oxide Nanofiltration Membrane Intercalated by Well-Dispersed Carbon Nanotubes for Drinking Water Purification. *Nanoscale* **2016**, *8*, 5696–5705. [CrossRef] [PubMed]
85. Ntim, S.A.; Mitra, S. Adsorption of Arsenic on Multiwall Carbon Nanotube–Zirconia Nanohybrid for Potential Drinking Water Purification. *J. Colloid Interface Sci.* **2012**, *375*, 154–159. [CrossRef] [PubMed]
86. Khalid, A.; Al-Juhani, A.A.; Al-Hamouz, O.C.; Laoui, T.; Khan, Z.; Atieh, M.A. Preparation and Properties of Nanocomposite Polysulfone/Multi-Walled Carbon Nanotubes Membranes for Desalination. *Desalination* **2015**, *367*, 134–144. [CrossRef]
87. Liu, Y.; Wu, P.; Liu, F.; Li, F.; An, X.; Liu, J.; Wang, Z.; Shen, C.; Sand, W. Electroactive Modified Carbon Nanotube Filter for Simultaneous Detoxification and Sequestration of Sb(III). *Environ. Sci. Technol.* **2019**, *53*, 1527–1535. [CrossRef] [PubMed]
88. Zarghami, S.; Mohammadi, T.; Sadrzadeh, M.; Van der Bruggen, B. Bio-Inspired Anchoring of Amino-Functionalized Multi-Wall Carbon Nanotubes (N-MWCNTs) onto PES Membrane Using Polydopamine for Oily Wastewater Treatment. *Sci. Total Environ.* **2020**, *711*, 134951. [CrossRef] [PubMed]
89. Jia, Z.; Kong, M.; Yu, B.; Ma, Y.; Pan, J.; Wu, G. Tunable Co/ZnO/C@MWCNTs Based on Carbon Nanotube-Coated MOF with Excellent Microwave Absorption Properties. *J. Mater. Sci. Technol.* **2022**, *127*, 153–163. [CrossRef]
90. Mukhtar, A.; Mellon, N.; Saqib, S.; Khawar, A.; Rafiq, S.; Ullah, S.; Al-Sehemi, A.G.; Babar, M.; Bustam, M.A.; Khan, W.A.; et al. CO_2/CH_4 Adsorption over Functionalized Multi-Walled Carbon Nanotubes; an Experimental Study, Isotherms Analysis, Mechanism, and Thermodynamics. *Microporous Mesoporous Mater.* **2020**, *294*, 109883. [CrossRef]
91. Seekaew, Y.; Wisitsoraat, A.; Phokharatkul, D.; Wongchoosuk, C. Room Temperature Toluene Gas Sensor Based on TiO_2 Nanoparticles Decorated 3D Graphene-Carbon Nanotube Nanostructures. *Sens. Actuators B Chem.* **2019**, *279*, 69–78. [CrossRef]

92. Sacco, L.; Forel, S.; Florea, I.; Cojocaru, C.-S. Ultra-Sensitive NO_2 Gas Sensors Based on Single-Wall Carbon Nanotube Field Effect Transistors: Monitoring from Ppm to Ppb Level. *Carbon N. Y.* **2020**, *157*, 631–639. [CrossRef]
93. Jeon, J.-Y.; Kang, B.-C.; Byun, Y.T.; Ha, T.-J. High-Performance Gas Sensors Based on Single-Wall Carbon Nanotube Random Networks for the Detection of Nitric Oxide down to the Ppb-Level. *Nanoscale* **2019**, *11*, 1587–1594. [CrossRef]
94. Yang, M.; Au, C.; Deng, G.; Mathur, S.; Huang, Q.; Luo, X.; Xie, G.; Tai, H.; Jiang, Y.; Chen, C.; et al. $NiWO_4$ Microflowers on Multi-Walled Carbon Nanotubes for High-Performance NH_3 Detection. *ACS Appl. Mater. Interfaces* **2021**, *13*, 52850–52860. [CrossRef]
95. Kaviyarasu, K.; Mola, G.T.; Oseni, S.O.; Kanimozhi, K.; Magdalane, C.M.; Kennedy, J.; Maaza, M. ZnO Doped Single Wall Carbon Nanotube as an Active Medium for Gas Sensor and Solar Absorber. *J. Mater. Sci. Mater. Electron.* **2019**, *30*, 147–158. [CrossRef]
96. Ma, L.; Dong, X.; Chen, M.; Zhu, L.; Wang, C.; Yang, F.; Dong, Y. Fabrication and Water Treatment Application of Carbon Nanotubes (CNTs)-Based Composite Membranes: A Review. *Membranes* **2017**, *7*, 16. [CrossRef]
97. Chowdhury, Z.Z.; Sagadevan, S.; Johan, R.B.; Shah, S.T.; Adebesi, A.; Md, S.I.; Rafique, R.F. A Review on Electrochemically Modified Carbon Nanotubes (CNTs) Membrane for Desalination and Purification of Water. *Mater. Res. Express* **2018**, *5*, 102001. [CrossRef]
98. Liu, Y.; Gao, G.; Vecitis, C.D. Prospects of an Electroactive Carbon Nanotube Membrane toward Environmental Applications. *Acc. Chem. Res.* **2020**, *53*, 2892–2902. [CrossRef] [PubMed]
99. Zhu, X.; Jassby, D. Electroactive Membranes for Water Treatment: Enhanced Treatment Functionalities, Energy Considerations, and Future Challenges. *Acc. Chem. Res.* **2019**, *52*, 1177–1186. [CrossRef]
100. Jain, N.; Gupta, E.; Kanu, N.J. Plethora of Carbon Nanotubes Applications in Various Fields—A State-of-the-Art-Review. *Smart Sci.* **2022**, *10*, 1–24. [CrossRef]
101. Omoriyekomwan, J.E.; Tahmasebi, A.; Dou, J.; Wang, R.; Yu, J. A Review on the Recent Advances in the Production of Carbon Nanotubes and Carbon Nanofibers via Microwave-Assisted Pyrolysis of Biomass. *Fuel Process. Technol.* **2021**, *214*, 106686. [CrossRef]

Disclaimer/Publisher's Note: The statements, opinions and data contained in all publications are solely those of the individual author(s) and contributor(s) and not of MDPI and/or the editor(s). MDPI and/or the editor(s) disclaim responsibility for any injury to people or property resulting from any ideas, methods, instructions or products referred to in the content.